

Meterwavelength Single-pulse Polarimetric Emission Survey II: The phenomenon of Drifting Subpulses

Rahul Basu¹, Dipanjan Mitra^{2,3,1}, George I. Melikidze^{1,4}, Krzysztof Maciesiak¹, Anna Skrzypczak¹, Andrzej Szary^{5,1}
rahul@astro.ia.uz.zgora.pl

ABSTRACT

A large sample of pulsars was observed as part of the Meterwavelength Single-pulse Polarimetric Emission Survey. We carried out a detailed fluctuation spectral analysis which revealed periodic features in 46% pulsars including 22 pulsars where drifting characteristics were reported for the first time. The pulsar population can be categorized into three distinct groups, pulsars which show systematic drift motion within the pulse window, the pulsars showing no systematic drift but periodic amplitude fluctuation and pulsars with no periodic variations. We discovered the dependence of the drifting phenomenon on the spin down energy loss (\dot{E}), with the three categories occupying distinctly different regions along the \dot{E} axis. The estimation of the drift periodicity (P_3) from the peak frequency in the fluctuation spectra is ambiguous due to the aliasing effect. However, using basic physical arguments we were able to determine P_3 in pulsars showing systematic drift motion. The estimated P_3 values in these pulsars were anti-correlated with \dot{E} which favoured the Partially Screened Gap model of Inner Acceleration Region in pulsars.

Subject headings: pulsars: general — pulsars:

1. Introduction

The pulsar radio emission consist of a sequence of highly periodic pulses occupying a small fraction of the pulsar period. The individual pulses are made up of one or more subpulses which, in some cases, exhibit systematic variation in position or intensity or both. This phenomenon is clearly seen in a pulse stack, which is an alternative representation of the pulsar data where consecutive pulsar periods are arranged on top of each other in a two dimensional array, with the horizontal axis along the pulse longitude and the vertical axis represent-

ing increasing period number. An impression resembling drift bands is seen in the pulse stack, first observed by Drake & Craft (1968), and is known as the phenomenon of drifting subpulses in pulsars, hereafter simply referred to as drifting.

The drifting greatly varies in the pulsar population and is broadly classified into two groups. The first corresponds to the phase modulated drifting where regular drift bands are seen. The second case is the amplitude modulated drifting where the subpulses are localised in the pulse window and only show periodic intensity variation. Around 35% of pulsars have been reported to show some form of drifting (Weltevrede *et al.* 2006, 2007). There are two periodicity associated with drifting, P_2 which measures the longitudinal separation between adjacent drift bands and P_3 the interval between the signal repeating at the same location (Backer 1970, 1973).

The drifting is closely related to the physical processes responsible for radio emission in pulsars. A force-free condition is believed to exist around

¹Janusz Gil Institute of Astronomy, University of Zielona Góra, ul. Szafrana 2, 65-516 Zielona Góra, Poland

²National Centre for Radio Astrophysics, Ganeshkhind, Pune 411 007, India

³Physics Department, University of Vermont, Burlington VT 05405

⁴Abastumani Astrophysical Observatory, Ilia State University, 3-5 Cholokashvili Ave., Tbilisi, 0160, Georgia

⁵ASTRON, the Netherlands Institute for Radio Astronomy, Postbus 2, 7990 AA, Dwingeloo, The Netherlands

the neutron star which introduces an electric field (\mathcal{E}) at a radial distance \mathbf{r} from the neutron star, which is represented in the observer's frame of reference as:

$$\mathcal{E} = -\frac{1}{c} (\boldsymbol{\Omega} \times \mathbf{r}) \times \mathbf{B}. \quad (1)$$

where $\boldsymbol{\Omega}(=2\pi/P)$ is the angular velocity of the neutron star and \mathbf{B} is the magnetic field. This further requires the formation of a charge separated magnetosphere with density $n_{\text{GJ}} = \boldsymbol{\Omega} \cdot \mathbf{B}/2\pi ec$ (Goldreich & Julian 1969), co-rotating with the neutron star. It should be noted that if the charge density goes below n_{GJ} , they no longer co-rotate with the neutron star, but lags behind the co-rotation with motion still around the rotation axis.

The pulsar magnetosphere is divided into two regions, the closed field line region and the open field line region, bounded by the light cylinder where the co-rotation speed is equal to the speed of light ($R_{\text{LC}} = c/\Omega$). The magnetosphere in the open field lines is initially charge starved, and a supply of charges can come from the neutron star surface or magnetic e^-e^+ pair production. An abundant supply of plasma ensures a flow of relativistic charged particles along the open field lines (Spitkovsky 2011). The pulsar radio emission is believed to originate as a result of the growth of instabilities in this outflowing plasma at a height of about 500 km above the neutron star surface (Mitra & Rankin 2002; Kijak & Gil 2003; Krzeszowski *et al.* 2009; Melikidze *et al.* 2000; Gil *et al.* 2004). The physical processes generating the relativistic plasma require the formation of a non-stationary inner acceleration region (IAR) in the immediate vicinity of the polar cap. The prototype for the IAR is the inner vacuum gap (IVG) first suggested by Ruderman & Sutherland (1975), hereafter RS75. They used magnetic fields of magnitude $\sim 10^{12}\text{G}$ calculated from slowdown rates corresponding to the dipolar component. However, significantly smaller values for the radius of curvature was used to determine the Lorentz factors of the relativistic charged particles in the gap implying non-dipolar components of magnetic field. The electric potential difference in the gap can accelerate positron/electron with energies $\sim 10^{12}\text{ eV}$. RS75 suggested that the gap breaks down as a result of pair production in high magnetic fields and subsequent acceleration in the electric fields which give rise to several equispaced sparking discharges.

The fully formed spark in the gap results in a non-stationary flow of plasma column and radio emission generated in this column is observed as a subpulse. It should be noted that the sparks, i.e. the regions of IAR where the local charge density differs from n_{GJ} , do not corotate with the pulsar. This lack of corotation in the sparks is manifested as the phenomenon of subpulse drifting in pulsars.

In recent years two methodologies have been used to probe the IAR, the X-ray emission from the polar caps and measuring the drift velocities (Gil *et al.* 2008). The thermal component of the X-ray emission revealed that the surface temperatures were lower than expected from the IVG of RS75. In certain pulsars the estimated drift velocities were less than the predicted RS75 values (see Deshpande & Rankin 1999; Gil *et al.* 2003a and references therein). This motivated Gil *et al.* (2003a) to propose the partially screened gap (PSG) model for the IAR.

In this paper, Meterwavelength Single-pulse Polarimetric Emission Survey-II (MSPESII), we have conducted an extensive study of drifting in the sample of pulsars from MSPES, the details of which are presented in section 2 (observation and analysis), 3 (primary results) and 4 (drifting properties). The inherent ambiguity in determining P_3 from the measured drifting feature due to the aliasing effect is discussed in section 5.1. In section 6 we have used basic physical arguments to determine P_3 in certain pulsars with interesting implications for the PSG model of the IAR.

2. Observation and Analysis

The details of the observing procedure of MSPES, using the Giant Meterwave Radio Telescope, was reported in Mitra *et al.* (2016), see table 1 therein. A total of 123 pulsars were observed in this survey with 118 pulsars at 618 MHz, 105 pulsars at 333 MHz and 100 pulsars at both these frequencies. The data were recorded in the full polarization mode, but we used only the total intensity single pulses for these studies¹. We used the fluctuation spectral analysis for determining the peri-

¹The pulsar J1703–3241 was observed on two occasions at 333 MHz, 2 March 2014 and 5 May 2014. MSPES uses data from 5 May due to proper polarization setting, we used 2 March data for MSPESII as the total intensity single pulses were found to be stronger.

odic features as described below. Some additional pre-processing of the data were also carried out as reported in appendix A.

2.1. Fluctuation Spectral Analysis

The most widely used technique for studying drifting is the Fluctuation Spectral analysis using the method of Fourier Transforms, where the peaks in the spectrum corresponds to the frequencies of drifting. There are three principal types reported in the literature, the Longitude Resolved Fluctuation Spectra (LRFS, Backer 1970), the Harmonic Resolved Fluctuation Spectra (HRFS, Deshpande & Rankin 2001) and the 2-Dimensional Fluctuation Spectra (2DFS, Edwards & Stappers 2002).

The LRFS involve selecting an appropriate number of consecutive pulses, n_s , and performing Discrete Fourier Transform (DFT) along each longitude in the pulse stack. The resultant complex fourier transform can be separated into two parts, the amplitude with peaks (f_p) representing the frequencies of periodic fluctuation (in units of cycles/ P), and the phase at f_p giving us a sense of subpulse variation across the pulse window.

The HRFS provides an alternate method of estimating the fluctuations in the pulsar signal and is useful in determining the nature of phase variation especially in less bright pulsars where the phase variation in the LRFS is not easily measured. In this technique one single DFT is carried out over the entire time series data, after padding the off-pulse region with zeros, i.e. a $n_s \times n_p$ DFT is carried out (n_p is the number of phase bins in every pulse period). The resultant one dimensional fourier transform is arranged as a function of the harmonic number (successive sections of $1/P$ cycles) to form the HRFS. In contrast to the LRFS, where f_p is mapped within the frequency range $0 - 0.5$ cycles/ P , the peaks in HRFS are mapped between $0 - 1.0$ cycles/ P . The extra frequency space ($0.5 - 1.0$ cycles/ P) in the HRFS provides direct realizations of the phase behaviour seen in the LRFS.

The 2DFS is an extension of the LRFS where additional Fourier Transform is performed along each horizontal axis of the LRFS. The adjacent drift bands are repeated at any longitude (ϕ) with a periodicity P_2 , implying a phase change of $\phi P/P_2$ across the longitudes. The estimation

of peaks along the horizontal axis of 2DFS gives a direct estimate of P_2 . Any f_p in the $-0.5 - 0$ cycles/ P frequency range of 2DFS is mapped in $0.5 - 1.0$ cycles/ P region of the HRFS.

We were primarily interested in estimating f_p using the fluctuation spectral technique (we used separate tools for estimating P_2 as explained below) and therefore used the LRFS and HRFS for our analysis. The n_s needed to carry out the LRFS/HRFS is ambiguous, but we found 256 pulses to be optimal for our studies. This number was high enough to obtain sufficient resolution in the frequency domain (0.004 cycle/ P), yet it was not too high such that the power in each frequency bin would be low for proper peak detection. In order to account for intrinsic intensity variation every 256 pulses used for fluctuation spectral analysis were folded to form a profile and all the 256 pulses subsequently normalised by the profile peak before the fluctuation spectral analysis. We searched for temporal variation in drifting using both LRFS and HRFS. The fluctuation spectra were determined as a function of time after shifting the start period by about 10 pulses and performing the DFT for each data set (a similar technique was also proposed by Serylak et al. 2009 for the 2DFS). The LRFS for each time realization was averaged along the longitude while the HRFS was averaged along the harmonic number and depicted in 2-dimensional maps with the vertical axis as the start period. The time varying fluctuation spectra in both cases were finally averaged across the time axis to determine the average frequency behaviour of the drifting signal which was used to determine f_p . The time averaged fluctuation spectra were normalised by the maximum value in spectra to make it independent of absolute flux. An example of our analysis is shown in figure 1, with the LRFS and HRFS (left panel, bottom and top respectively) as well as their time variations (right panel).

2.2. Determining f_p

The time averaged LRFS and HRFS were used to determine the frequency peaks of fluctuation as described below:

1. The fluctuation spectra was divided into five sections and a mean and rms was determined for each. The section with the minimum rms was identified as the baseline with its mean (μ_f) and

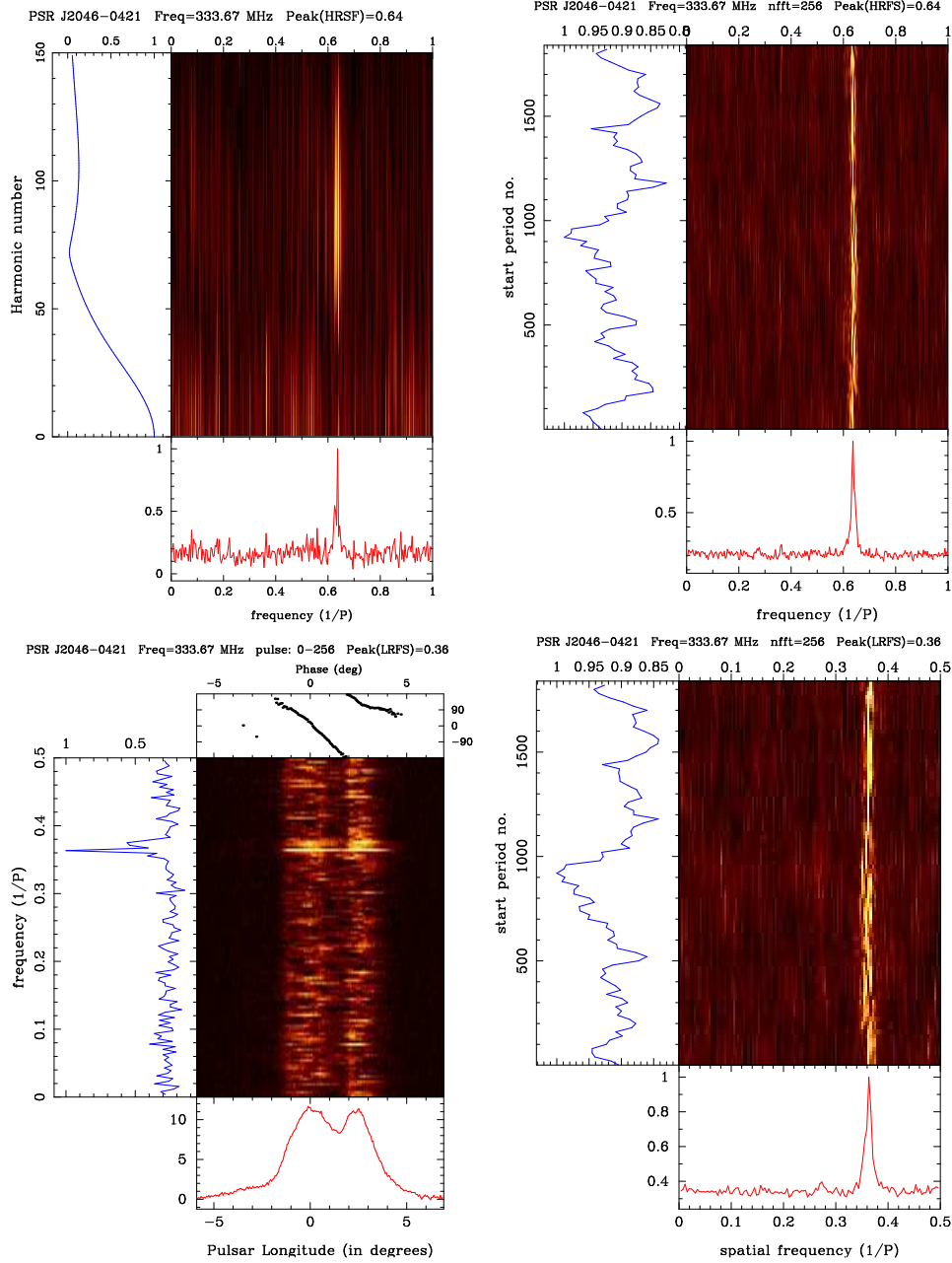


Fig. 1.— The fluctuation spectral analysis for the pulsar J2046-0421. The LRFS (bottom left) and the HRFS (top left) is shown for the pulse sequence 0-256. The LRFS also shows the phase variation across the pulse window at the peak amplitude. The time variation of the LRFS (bottom right) and the HRFS (top right) was used to determine the peaks. The LRFS in this example show a narrow peak at $f_p = 0.363$ cycle/ P and the phase at the peak vary with a negative slope across the pulse window. The corresponding peak in the HRFS is shifted to $\tilde{f}_p = 0.637$ cycle/ P , $(1-f_p)$, which is another indication of the negative slope of phase variation.

rms (σ_f) used as baseline characteristics.

2. All regions in the spectra with at least 3 consecutive points in excess of $\mu_f + 5\sigma_f$ were identified as potential structures. In case of wider structures the points going below the cutoff level was also included provided they were bordered by values in excess of the cutoff level.

3. The peak frequency was determined as the centroid of the above identified regions (Weltevrede *et al.* 2006):

$$f_p = \frac{\sum V_f \times f}{\sum V_f}, \quad (2)$$

here V_f is the fluctuation spectra value at frequency f .

4. The Full Width at Half Maximum ($FWHM$) for each peak, around the region identified for peak measurement, was calculated and used to estimate the rms level (gaussian approximation):

$$\sigma_p = \frac{FWHM}{2\sqrt{2} \ln 2} \approx \frac{FWHM}{2.355} \quad (3)$$

5. The error in f_p was estimated as (Kijak & Gil 1997):

$$\Delta f_p = \sigma_p \sqrt{1 + \left(\frac{\sigma_f}{V_p - \mu_f} \right)^2} \quad (4)$$

Here V_p is the value of the fluctuation spectra at f_p .

2.3. Determining P_2

The P_2 can be measured unambiguously if there are more than one drift band seen in a given single pulse, making it viable in a small subset of pulsars. A direct method is to measure separation between the subpulses, corresponding to adjacent drift bands, from strong single pulses. An enhancement to this approach was devised in order to increase the signal to noise ratio. The peaks in the pulse window for all significant single pulses ($> 5\sigma_N$, σ_N the rms of off-pulse region) were determined. A narrow window in the pulse longitude (3-5 bins) was selected and all the single pulses with peak within this window were averaged to form a folded profile with well separated subpulses. The selected window was shifted continuously across the entire pulse window to generate multiple profiles. The separation between the

peaks of adjacent subpulses in each profile (if more than one peak was visible) was measured. P_2 was determined after averaging the measured separation from all profiles. The error in P_2 is given as $\Delta P_2 = \Delta\phi \sqrt{1 + (\sigma_P/V_P)^2}$, here $\Delta\phi$ is the resolution of profile, σ_P the rms in the off pulse region of the average profile and V_P the peak value of average profile. In figure 2 we show the result of these exercises for the pulsar J2046–0421. Three peak-folded sub profiles are shown in the figure (red, green and blue profiles) as well as the full profile from all single pulses (in black). As seen in the figure the profiles in red and blue has well separated subpulses and all such profiles were used for estimating P_2 . The green profile has just one detectable peak and hence could not be used for these calculations.

3. Results

The analysis techniques described in the previous section were implemented using software packages developed for this work and applied to the 123 pulsars in MSPES. The pulsars showing drifting are listed in Table 1. In Table ?? we report the detected peaks in time average LRFS and HRFS for each pulsar. All significant peaks along with P_2 (if applicable) are also listed in the table.

3.1. Summary of Results

1. 57 pulsars has features with measurable peaks, i.e. 46% of pulsars in our sample show drifting.

2. Drifting is seen for the first time in 22 pulsars and verified in further 35 cases. There are around 100 pulsars with drifting reported in the literature (Gil *et al.* 2006). Our present survey substantially increases this population by 20%. The references for previous studies of drifting in individual pulsars are listed in table 1.

3. We have detected drifting in 38 pulsars at 333 MHz, 44 pulsars at 618 MHz and 25 at both frequencies.

4. P_2 is measured in 10 pulsars, i.e. around 18% of the pulsars with drifting.

5. In 28 pulsars the periodic features show non zero phase variations, 9 of which are new detec-

Table 1: List of Pulsars with Drifting features

Phase Modulation			Amplitude Modulation			No Detection	
New Detection	Previously Reported		New Detection	Previously Reported		PSR	Ref.
PSR	PSR	Ref.	PSR	PSR	Ref.		
J0846–3533	J0034–0721	1, 2, 3, 4, 5, 6	J1034–3224*	J0758–1528	5	J0820–4114	10, 11
J0959–4809	J0151–0635	4, 5, 7	J1116–4122	J0837+0610	4, 5, 15, 16	J0922+0638	4, 5
J1418–3921	J0152–1637	4, 5	J1328–4921	J1239+2453	4, 5, 19, 20, 21	J0953+0755	5, 17, 18
J1527–3931	J0304+1932	4, 5, 8, 9	J1603–2531	J1645–0317	4, 5, 22, 23	J1607–0032	4, 5
J1555–3134	J0525+1115	4, 5	J1604–4909	J1733–2228	5	J1820–0427	5
J1703–3241	J0630–2834	4, 5	J1625–4048	J1735–0724	5	J1847–0402	5
J1700–3312	J0820–1350	4, 5, 12, 13, 14	J1722–3207	J1740+1311	5, 24, 25	J1849–0636	4, 5
J1816–2650	J0944–1354	5	J1733–3716	J1842–0359	5	J1913–0440	4
J1919+0134	J1041–1942	4, 5	J1741–3927	J1848–0123	4, 26	J1941–2602	4
	J1720–2933	4, 5	J1748–1300	J1900–2600	4, 5, 27	J2346–0609	4
	J1741–0840	4, 5	J1801–0357	J1909+1102	5		
	J1822–2256	4, 5, 6	J1801–2920	J1919+0021	4, 5		
	J1901–0906	4, 5	J2006–0807	J1932+1059	4, 5, 29, 30, 31		
	J1921+1948	5, 26, 28		J1946+1805	4, 5, 6, 32, 33		
	J1921+2153	4, 5, 19		J2048–1616	4, 5, 22, 30, 34		
	J2046–0421	4, 5		J2330–2005	5		
	J2046+1540	4, 5					
	J2305+3100	4, 5, 35, 36					
	J2317+2149	5					

* the phase change was indeterminate;

References: 1-Huguenin *et al.* 1970; 2-Vivekanand & Joshi 1997; 3-Smits *et al.* 2005; 4-Weltevrede *et al.* 2006; 5-Weltevrede *et al.* 2007; 6-Serylak *et al.* 2009; 7-Biggs *et al.* 1985; 8-Schönhardt & Sieber 1973; 9-Backer *et al.* 1975; 10-Bhattacharyya *et al.* 2007; 11-Bhattacharyya *et al.* 2009; 12-Biggs *et al.* 1987; 13-Janssen & van Leeuwen 2004; 14-Lyne & Ashworth 1983; 15-Sutton *et al.* 1970; 16-Asgekar & Deshpande 2005; 17-Backer 1970; 18-Wolszczan 1980; 19-Proszynski & Wolszczan 1986; 20-Srostlik & Rankin 2005; 21-Maan & Deshpande 2014; 22-Taylor & Huguenin 1971; 23-Taylor *et al.* 1975; 24-Rankin *et al.* 1988; 25-Force & Rankin 2010; 26-Hankins & Wolszczan 1987; 27-Mitra & Rankin 2008; 28-Rankin *et al.* 2013; 29-Oster *et al.* 1977b; 30-Nowakowski *et al.* 1982; 31-Backer 1973; 32-Deich *et al.* 1986; 33-Kloumann & Rankin 2010; 34-Oster & Sieber 1977a; 35-Sieber & Oster 1975; 36-Redman *et al.* 2005.

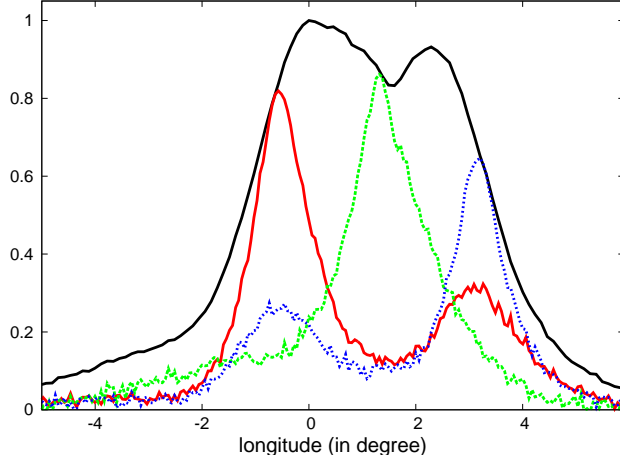


Fig. 2.— The figure shows the Peak folding method for estimating P_2 in pulsar J2046–0421. The single pulses with peaks within a narrow window (5 bins) are averaged to form profile with separated subpulses. The window is shifted across the pulse longitudes from the leading to the trailing edge to form multiple profiles. Three such examples are shown in the figure, the red profile with peak near the leading edge, the green profile with peak near the central region and the blue profile with peak near the trailing edge, with the average profile in black. The red and blue profiles have well separated subpulses and can be used to determine the separation between subpulse peaks. The estimated P_2 is the mean of all such separations that can be measured. The estimated P_2 for PSR J2046–0421 is $3.37 \pm 0.06^\circ$.

tions.

6. In 29 pulsars the periodic features are associated with no phase variation, 13 of which are reported for the first time.

7. There are 10 pulsars where drifting has been reported in the past but our analysis failed to detect any such features. In most cases this could be traced to the presence of RFI or low level features below our detection threshold.

3.2. Classification of Drifting Features

3.2.1. The strength of Drifting feature

The drifting was classified by Weltevrede *et al.* (2006) in terms of the width of the features, narrow widths (< 0.05 cycles/ P) were labeled as coherent drifters while wider features (> 0.05 cycles/ P) were called diffuse drifters. This classification scheme do not include any quantitative information about the relative strength of the features. We have devised an updated scheme for quantifying drifting using the quantity S which is

defined as the ratio between the peak height and effective width of the feature;

$$S = \frac{V_p - \mu_f}{FWHM}, \quad (5)$$

here V_p is the measured value at f_p , μ_f the mean baseline level and $FWHM$ is the Full Width at Half Maximum of the drifting feature. We determined S_L and S_H for all peaks measured from the time averaged LRFS and HRFS (table ??). The normalisation of the fluctuation spectra (see section 2.1) ensured that the estimated S is independent of the large scale intensity fluctuation as well as the absolute flux of the pulsar.

3.2.2. The Phase behaviour

The drifting can be classified into different categories based on the nature of subpulse motion across the pulse window. This is reflected in the phase behaviour seen at the peak frequency in LRFS, either showing large phase variation or very little change in phase across the pulse window. Sometimes, the periodic features are too weak with no phase measurements possible. In

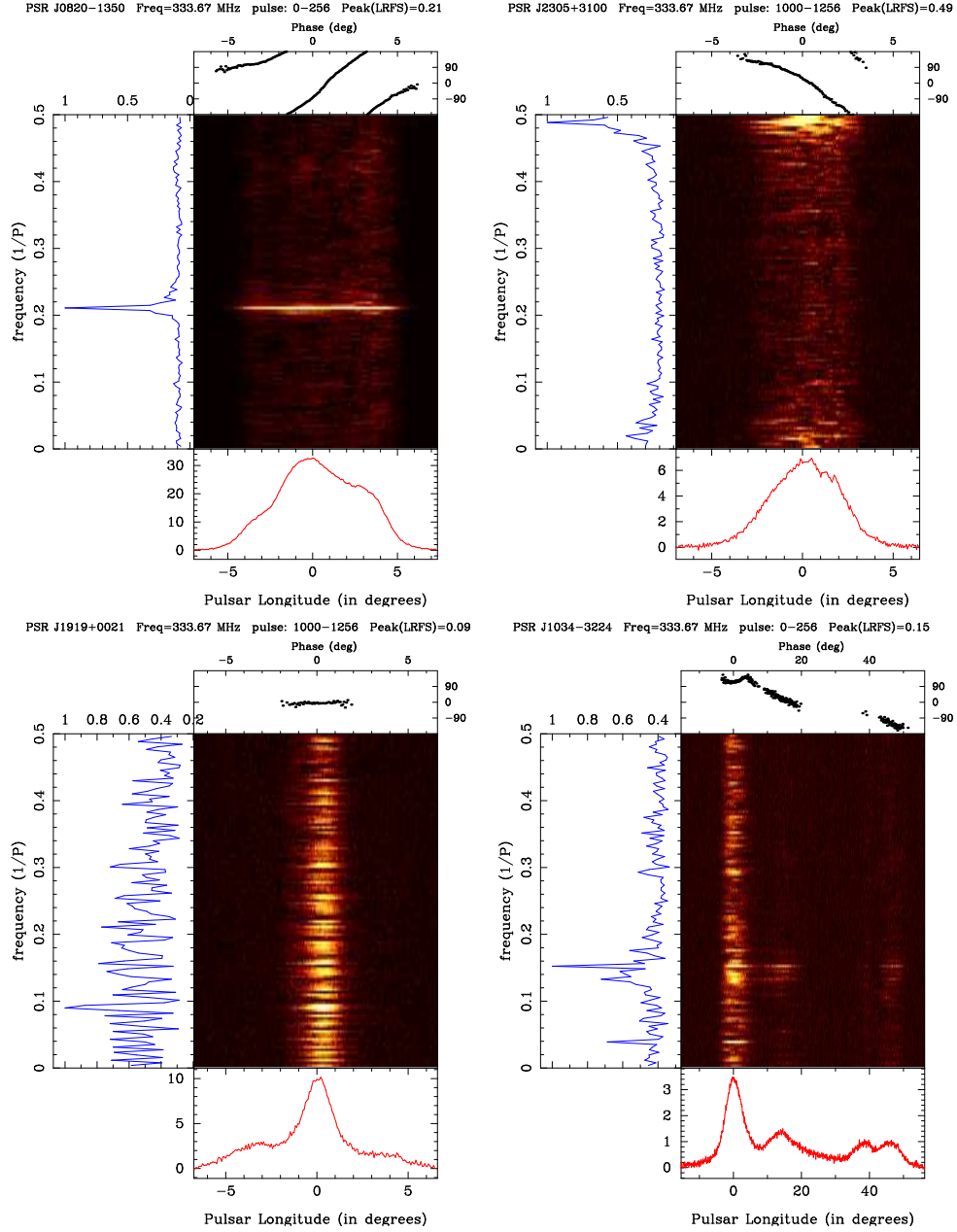


Fig. 3.— The figure shows the LRFS corresponding to the four different configurations of drifting based on the phase behaviour. The pulsar J0820-1350 (top left panel) belongs to the class Negative Drifting (ND) where the phase show a positive slope as it changes across the pulse window. The pulsar J2305+3100 (top right panel) is an example of Positive Drifting (PD) with the phase showing a negative slope from the leading to the trailing edge. In case of pulsar J1919+0021 (bottom left panel) no phase change seen across the profile which is an example of Amplitude Modulated Drifting (AMD). The pulsar J1034-3224 (bottom right panel) show a complicated phase behaviour which cannot be classified into the three categories.

these cases the HRFS can be used to decipher the phase nature as it shows different behaviour for each case. Based on the phase behaviour we have divided the drifting population into three groups which we describe below.

Negative Drifting (ND): This category of pulsars exhibit phase variation across the pulse window which show a positive slope from the leading to the trailing edge of the profile. This is exemplified by the pulsar J0820–1350 in figure 3. The ND is seen in the pulse stack as subpulses shifting towards the leading edge of the profile. The HRFS has a unique response for the ND, with the peaks in the LRFS having identical locations in the HRFS as well, i.e the HRFS have peaks in the $0 - 0.5$ cycles/ P range.

Positive Drifting (PD): In this scenario the phase across the pulse window changes with a negative slope from the leading to the trailing edge of the profile, as seen in pulsar J2305+3100 (see figure 3). The subpulses show a gradual shift towards the trailing edge. The peaks in the HRFS is reflected in case of PD, with any f_p in LRFS seen at $\bar{f}_p (=1-f_p)$ in the HRFS, i.e. the HRFS peak lies in the $0.5 - 1$ cycles/ P range.

Amplitude Modulated Drifting (AMD): The AMD corresponds to pulsars where the subpulses do not move across the pulse window but exhibit periodic change in intensity. The phases across the pulse window do not show much change and mostly remains flat with near zero slope as seen in pulsar J1919+0021 (figure 3). Any f_p seen in LRFS appears at two locations corresponding to f_p and \bar{f}_p in the HRFS with equivalent S .

The phase behaviour in pulsar J1034–3224 (figure 3) is complicated without any clear trend. The leading component of the profile shows a slightly positive slope which abruptly changes to a more pronounced negative slope in the later components. The peaks in the HRFS is similar to the AMD case with two prominent peaks having equivalent S . We have not classified this pulsar under any of the three schemes.

It should be noted that the three cases described above correspond to different morphologies of the pulsar profile (Rankin 1986, 1993). The

ND and PD belong to the category of phase modulated drifting and is mostly seen in pulsars which have conal components and are typically classified as conal single or double. The AMD is usually found in pulsars with core components. Table 1 lists the ND and PD as phase modulated drifting and AMD under amplitude modulation. In table ?? we have indicated the phase nature of drifting in each pulsar.

4. Physical Properties

4.1. Frequency Dependence

The separate measurements at two frequencies, 333 MHz and 618 MHz, allowed us to investigate the frequency dependence of drifting. There were 100 pulsars observed at the two frequencies out of which 25 pulsars showed drifting at both frequencies. 12 pulsars exhibited drifting at 333 MHz and not 618 MHz while 9 pulsars only at 618 MHz.

We were able to measure P_2 at both frequencies in 7 pulsars. In order to understand the frequency dependence of P_2 , we determined the ratio between 618 MHz and 333 MHz and plotted it as a function of 333 MHz value (figure 4, left panel). The 618 MHz measurements were usually lower than the 333 MHz value with an average ratio of ~ 0.89 (dashed horizontal line). This is consistent with the radius to frequency mapping which states that the pulse width and component separation decreases with increasing frequency. Assuming a power law dependence of P_2 on frequency, $P_2 \propto \nu^a$, the spectral index was $a \sim -0.19 \pm 0.04$. The spectral index matched the frequency dependence of pulse width reported in MSPES.

We also explored the frequency evolution of f_p in the 25 pulsars where dual frequency measurements were available. We once again determined the ratio between 618 MHz and 333 MHz and plotted them as a function of the 333 MHz value (figure 4, right panel). In the figure the horizontal line is drawn around unity and all ratios, within errors, fall on this line. This agrees with previous studies by Nowakowski *et al.* (1982); Weltevrede *et al.* (2007) which claim drifting to be a broadband phenomenon independent of observing frequency.

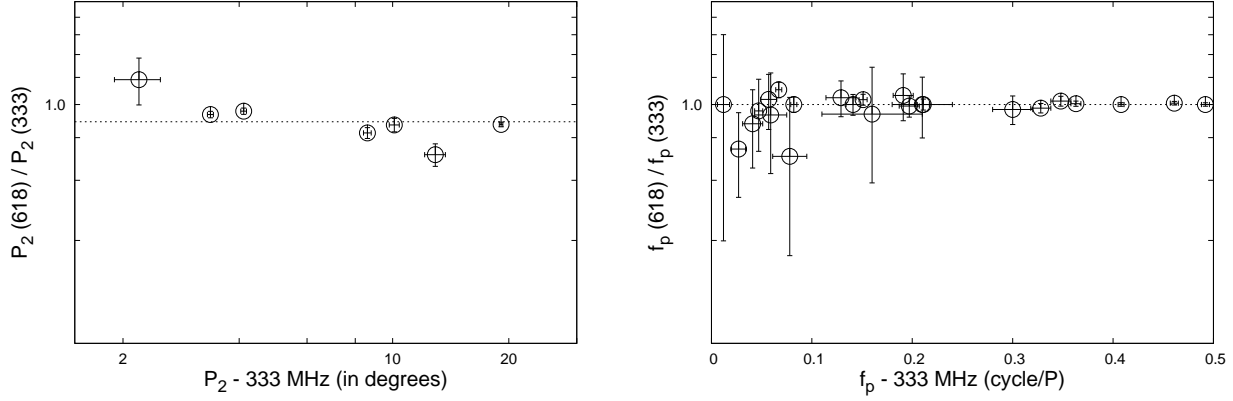


Fig. 4.— The figure shows the frequency dependency of P_2 (left panel) and f_p (right panel). In each case we plot the ratio of 618 and 333 MHz measurement as a function of 333 MHz value. The horizontal (dashed) line in the left panel corresponds to the best fit value 0.89 implying that the P_2 at 618 MHz is lower than 333 MHz. This is expected from radius to frequency mapping where the profile width and component separation decreases with increasing frequency. The horizontal (dashed) line on the right panel is set at 1 and shows that within errors the measurements at the two frequencies are identical.

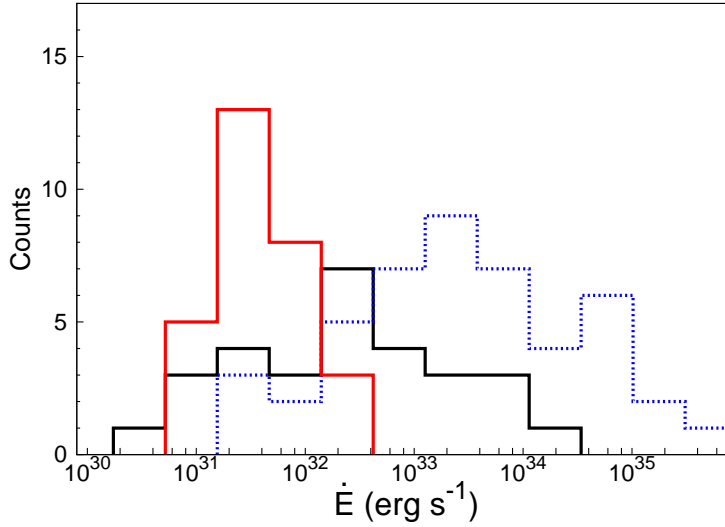


Fig. 5.— The figure shows the distribution of spin-down energy loss (\dot{E}) for the pulsars used for drifting studies. The histograms are shown for the three distinct populations, the pulsars without any periodic features (dotted blue line), the pulsars showing phase stationary amplitude modulation (solid black line) and the pulsars exhibiting phase modulations (solid red line). Pulsars without any periodic features tend to have higher \dot{E} compared to pulsars which show drifting. The figure also shows that the phase modulated drifting is seen only in a narrow range of $\dot{E} < 10^{33}$ erg s⁻¹.

4.2. Distribution with Spin down Energy loss

We estimated the distribution of the three groups of pulsars based on drifting behavior, phase modulated drifting (ND and PD), amplitude modulated drifting (AMD) and no drifting, as a function of the spin down energy loss (\dot{E}) as shown in figure 5. The phase modulated distribution with 28 pulsars is represented in red histograms and occupy a very narrow region in the lower \dot{E} range, between 10^{30} - 10^{33} erg s $^{-1}$, with peak around 10^{31} erg s $^{-1}$. The amplitude modulation case with 28 pulsars, shown as black histograms, has a much wider distribution peaking around 10^{32} erg s $^{-1}$ and declines beyond 5×10^{34} erg s $^{-1}$. The pulsars which do not show drifting is depicted by the blue dotted histograms. We have excluded the pulsars with no detectable single pulses (see MSPES) and the 10 pulsars in table 1 with previously reported drifting but not detected in our analysis, leaving 46 pulsars in this distribution. The distribution peaks around $\dot{E} \sim 10^{33}$ erg s $^{-1}$ and tends toward the higher \dot{E} range with a lower cutoff around 10^{31} erg s $^{-1}$. It should be noted that our sample selection criterion in MSPES favours lower \dot{E} ($< 10^{36}$ erg s $^{-1}$) pulsars which will likely skew this distribution.

We explored the statistical difference between the three distributions using the Student's t-test which indicate the probability that two independent samples of data are from the same population by estimating the mean of each distribution and calculating a 't' value which is the weighted difference of the means (Press *et al.* 1992). To apply the above method we collected the three distributions taking the logarithm of the \dot{E} value for every pulsar. The 't' value was 3.75 for the phase modulated and amplitude modulated sample with a corresponding probability of 6.3×10^{-4} for the two to be from the same distribution. Here, a probability of 1 corresponds to the two datasets being identical and 0 corresponds to no overlap. The corresponding values between the phase modulated sample and the not drifting pulsars were 't' value of 10.67 and a likely overlap probability of 10^{-6} . For the amplitude modulated and not drifting pulsars the 't' value was 4.12 and the probability of overlap was 1.2×10^{-4} . The analysis indicate that it is very likely that the means of the three distributions were very different. It is remarkable to

note that pulsars separate out into three distinct populations based on drifting behaviour along the \dot{E} axis.

Similar exercises were also carried out with other pulsar parameters P , the spin down rate (\dot{P}) and characteristic age (τ), but no clear difference was seen between the three drifting populations along any of these parameters.

5. Drifting Periodicity

5.1. Alias Effect

The fluctuation spectral analysis measures the different frequencies associated with drifting characterised by f_p in the LRFS. The different models for the emission mechanism in pulsars are mostly concerned with the drift periodicity P_3 , which is the interval between subpulses to repeat at the same location in the pulse window. As mentioned earlier, in certain models the subpulse drift phenomenon is associated with drifting of sparks in the IAR. The P_3 is then used to estimate the drift velocity of sparks in the IAR and hence is important for understanding the physical conditions in the pulsar magnetosphere. There is however the aliasing effect that is responsible for uncertainty in estimating the actual P_3 from the measured f_p , i.e P_3 is not simply $1/f_p$, owing to certain limitations of observations. The pulsed emission is visible for a short duration every period which makes any measured frequency subject to certain restrictions. This ensures that f_p , in LRFS, at any longitude is only measured in the frequency range 0 - 0.5 cycles/ P . The aliasing effect ensures that any periodicity outside this frequency range will be folded into the above domain.

The aliasing effect associated with f_p is whether the measured frequency is the actual frequency or the reflection of the larger fundamental frequency in the measured window. This means that for any actual frequency, $f_p^a > 0.5$ cycles/ P , the measured f_p will be different. The two frequencies are related as (Gupta *et al.* 2004)

$$f_p^a = 2k \times 0.5 + (-1)^l f_p \quad (6)$$

Here, $k = INT[(n+1)/2]$ and $l = mod(n, 2)$, with n being the alias order, $n \times 0.5 < f_p^a < (n+1) \times 0.5$ cycles/ P .

We explore one manifestation of aliases arising as a result of subpulse motion across the pulse

window and the drift direction. The pulsar signal is not restricted to a single longitude but spread over a finite window, characterised by the profile width. This implies that for a given choice of f_p there is an inherent ambiguity in the direction of subpulse motion, i.e. whether the subpulses are moving from the leading to the trailing edge of the profile or in the opposite direction. To illustrate this we note that the ND correspond to the subpulses in subsequent periods appearing at earlier longitudes, and the PD is seen when the subpulses appear at later longitudes. If the subpulses are intrinsically moving from the trailing to the leading edge of the profile, ND would correspond to the actual peak being f_p ($0 < f_p < 0.5$ cycles/ P) while PD would imply the actual peak to be $\bar{f}_p (=1-f_p, 0.5 < \bar{f}_p < 1$ cycles/ P). The opposite is true if the subpulses are moving from the leading to the trailing edge, ND would correspond to \bar{f}_p while PD would correspond to f_p . Unfortunately, any observation of the pulse window gives a snapshot of the subpulse structure with no way to estimate their actual direction of motion. In appendix B we have simulated single pulses to highlight the degeneracy associated with drift direction. The salient features of the aliasing problem based on the direction of subpulse motion is summarized in table 2.

5.2. Determining P_3

As argued above the actual drifting periodicity is intrinsically indeterminate, especially whether f_p is the actual frequency or a reflection of the larger fundamental frequency in the measured window. Hereafter, we assume the measured f_p to be the fundamental frequency which physically corresponds to the frequency of spark repetition. In case of the phase modulated drifting (ND and PD) it is possible to determine the alias between P and $2P$ if the direction of subpulse motion is known as we discuss below. As discussed in the introduction the subpulse motion is closely linked to the sparks formed in the IAR. The sparks in the IAR has a specific direction, lagging behind the co-rotation of the neutron star. Every subsequent period, as the pulsar comes within our field of view, the spark associated plasma are lagging behind and gives an impression of moving opposite to the co-rotation. If the above hypothesis is correct we have a preferred direction for drifting.

The corotation direction is intrinsically from the leading to the trailing edge of the profile, which implies that the subpulses are expected to move in the opposite direction, i.e from the trailing to the leading edge. As explained in table 2, this gives a preferred periodicity for the phase modulated drifting, ND with $P_3 = 1/f_p$ and PD with $P_3 = 1/(1-f_p)$. In other words the drift periodicity is reflected in the peaks of the HRFS. We have determined the unaliased P_3 values in the phase modulated pulsars as shown in table ??, which also lists the unresolved $P_3 = 1/f_p$ for the amplitude modulated cases. In each P_3 measurement we used the weighted average of the f_p measurements from the two frequencies. The error is estimated as $\delta P_3 = \delta f_p / f_p^2$.

The definition of P_3 in this work is different from many studies in the literature where the drifting even in non-aligned pulsars is believed to originate as a result of circulating beamlets around the magnetic axis (Gil & Sendyk 2000). In our assumption of drifting the direction of subpulse motion is independent of whether the line of sight is along the inner or outer² region of the emission beam. This is contrary to the assumptions in other works, e.g. Deshpande & Rankin (1999); Weltevrede *et al.* (2006, 2007), where the inner and outer line of sights have opposite directions of subpulse motion. As a result most of these works estimate $P_3 = 1/f_p$ for both the ND and PD (Weltevrede *et al.* 2006, 2007) cases with the direction of drifting associated with the inner or outer line of sight. To summarize, our estimation of P_3 is identical to Weltevrede *et al.* (2006, 2007) for ND and AMD pulsars. In case of PD pulsars our estimations $P_3 = 1/(1-f_p)$ ($P < P_3 < 2P$) while Weltevrede *et al.* (2006, 2007) uses $P_3 = 1/f_p$ ($P_3 > 2P$).

6. Effect of Pulsar Parameters on P_3

6.1. Dependence on \dot{E}

We have determined the variation of P_3 (in units of pulsar period P) as a function of \dot{E} ergs/s, as shown in figure 6. The ND is represented with red

²The inner line of of sight, often called as negative β is when the observer cuts the emission beam between the rotation axis and the magnetic axis, and outer line of sight, or positive β is when the sightline cuts the beam outside the rotation and magnetic axis.

Table 2: Schematic of Aliasing associated with Drift direction.

Drifting Type	1 st alias ($P_3 > 2P$)	2 nd alias ($P_3 < 2P$)
Negative Drifting (ND)	subpulse from trailing to leading edge	subpulse from leading to trailing edge
Positive Drifting (PD)	subpulse from leading to trailing edge	subpulse from trailing to leading edge
Amplitude Modulation (AMD)	line of sight at lower part of subpulse	line of sight at upper part of subpulse

The pulsar rotation direction is from the leading to the trailing edge.

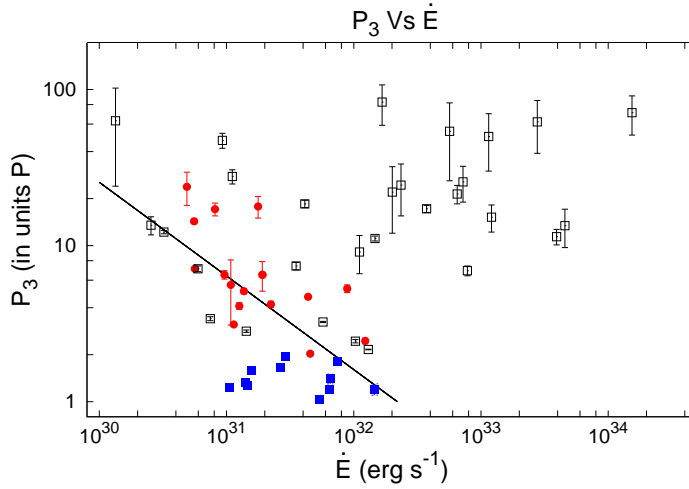


Fig. 6.— The figure shows the variation of the predicted drifting periodicity P_3 as a function of the spin-down energy loss (\dot{E}). The three different populations of periodic features are colour coded, with the red dots corresponding to positive phase drifting ($P_3 > 2P$), the blue squares representing the negative phase drifting ($P_3 < 2P$), and the open black squares associated with the amplitude modulated drifting ($P_3 > 2P$, aliasing cannot be resolved). The phase modulated drifting (red and blue points) show an anti-correlation with \dot{E} . The phase modulated drifting is not seen for $\dot{E} > 10^{33} \text{ erg s}^{-1}$, which is also the region where the anti-correlation expects P_3 to go below P .

dots, the PD with blue squares and the AMD with black open square symbols. The phase modulated drifting show an anti-correlation between P_3 and \dot{E} with a correlation coefficient of -0.7 . The anti-correlation indicates that the expected $P_3 < P$ for $\dot{E} > 10^{33} \text{ erg s}^{-1}$. This is a likely explanation for the absence of phase modulated drifting at the high \dot{E} regime. In order to determine the relationship between P_3 and \dot{E} a fit was sought (Press *et al.* 1992) with the functional relationship

$$P_3 = \left(\frac{\dot{E}}{\dot{E}_0} \right)^\delta \quad (7)$$

The best fit values corresponded to $\dot{E}_0 = 2.3 \pm 0.2 \times 10^{32} \text{ erg s}^{-1}$ and $\delta = -0.6 \pm 0.1$ and is represented by the black line in figure 6.

6.2. Implications for Physical Models

The key assumption that allowed us to plot figure 6 is that subpulse drifting results due to lack of corotation of sparks, with the velocity of the sparks lagging behind the corotation velocity. In this section we explore different IAR models that provide this circumstance.

6.2.1. The inner vacuum gap model of RS75

The lack of corotation of sparks was primarily put forward by RS75, where they estimated the spark repeating timescale P_3 , based on two assumptions 1. they considered an anti-pulsar system, where the pulsar rotation axis and the magnetic axis are exactly aligned, but are opposite to each other, 2. and that a number of sparks n_{sp} rotate around the rotation axis (and hence for an aligned rotator the sparks rotation is also around the magnetic axis) in a circular path around the circumference of the polar cap, where the circulation time of each spark was given as $\hat{P}_3 = n_{\text{sp}} \times P_3$.

This led RS75 to find $P_3 \simeq (5.6/n_{\text{sp}}) B_{12}/P^2$ (equations 33 and 34 in RS75), where B_{12} is the magnetic field in units of 10^{12} G . The dependence of \dot{E} on P_3 in RS75 model can be found by using the dipolar magnetic field as $B = 3.2 \times 10^{19} (PP)^{0.5} \text{ G}$ with the spin down energy loss, $\dot{E} = 4\pi^2 I(\dot{P}/P^3)$, where $I \simeq 10^{45} \text{ gm cm}^2$, is the moment of inertia of the neutron star. The

dependence is given as

$$P_3 \simeq \frac{5.6}{n_{\text{sp}}} \left(\frac{\dot{E}}{\dot{E}_1} \right)^{0.5}. \quad (8)$$

Here P_3 is expressed in units P , n_{sp} corresponds to the number of sparks in the IVG and $\dot{E}_1 \simeq 4 \times 10^{31} \text{ erg s}^{-1}$.

Applying the above dependence of P_3 with \dot{E} to figure 6 is difficult since P_3 in equation 8 is derived for an aligned rotator which does not correspond to a real pulsar. In the non-aligned case if drifting is related to sparks that only lag the corotation velocity then the direction of the spark velocity only lags behind the observers line of sight or in other words the drift motion is around the rotation axis. An external observer would essentially see that the sparks are drifting across the polar cap, and as a consequence equation 8 which is derived by calculating the spark circulation time around the polar cap cannot be used to calculate P_3 . In fact, if the requirement for the drifting phenomenon is that the spark has to lag behind corotation, then a circular motion around the polar cap for a non-aligned pulsar will contradict our basic assumption as parts of the spark motion in the polar cap will lag the corotation velocity while there will be parts which will be leading.

6.2.2. Partially Screened Gap Model

We now discuss the IAR model of subpulse drifting for a real pulsar, i.e. for a non-aligned case, where the spark moves along the locus of the observers line of sight at a velocity which is slower than the observers line of sight velocity. Further, based on several observational constraints as discussed in the introduction, we will invoke the model where the IAR is a PSG. The PSG model differs from the IVG by considering a steady flow of ions from the stellar surface which screens the accelerating electric field of the gap by a screening factor η (where $\eta = 1 - \rho_i/\rho_{\text{GJ}}$, ρ_i is the density of ions in IAR and ρ_{GJ} is the Goldreich-Julien density; Gil *et al.* 2003a). One simple way of realising the effect of η on the velocity of sparks is the following. The magnitude of the corotational velocity $v_{\text{cr}} = (E/B)c$, where E and B correspond to the electric and magnetic field in the IAR. The effect of η is to reduce the electric field in the gap such that the real drift velocity of the sparks $v_r \approx \eta v_{\text{cr}}$.

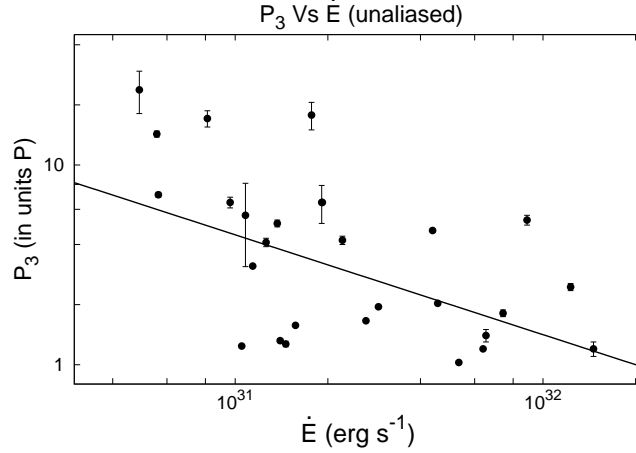


Fig. 7.— The figure shows the estimated P_3 of pulsars showing phase modulated drifting as a function of \dot{E} . The black line corresponds to equation 12 which gives the behaviour of P_3 with \dot{E} as given by the PSG model (see section 6.2.2 for further details)

Next we will conjecture that the PSG at any given time is packed with a number of circular sparks, where the size of a spark and the space between the sparks is h . This implies that the distance between the centers of two adjacent sparks is $2h$. The sparks move along the line of sight of the observer, and hence the spark repeating time at any given longitude is estimated as $P_3 = 2h/v_d$. It can be shown that if screening factor η is small (~ 0.1) then P_3 is given as:

$$P_3 = \frac{1}{2\pi \cos(\alpha)} \frac{1}{\eta} \quad (9)$$

Here, α is the angle between the magnetic and rotation axis (see equation 3.55 Szary 2013).

To find a relation between P_3 and \dot{E} in the PSG model, we first note that the full energy outflow from the polar cap can be expressed as:

$$L_{\text{PSG}} \simeq \gamma_0 m_e c^3 \eta n_{\text{GJ}} A_{\text{pc}}. \quad (10)$$

Here γ_0 is a characteristic Lorentz factor of electrons or positrons accelerated in the gap, n_{GJ} is GJ particle density and A_{pc} is the area of the polar cap surface. Let us note that the value of $n_{\text{GJ}} A_{\text{pc}}$ does not depend on the surface magnetic field configuration due to the magnetic flux conservation law. We can estimate $n_{\text{GJ}} \simeq 7 \times 10^{10} \cos(\alpha) (\dot{P}_{-15}/P)^{0.5} \text{ cm}^{-3}$

and $A_{\text{pc}} \simeq 3 \times 10^8 P^{-1} \text{ cm}^2$ for the dipolar polar cap which gives an invariant value of $n_{\text{GJ}} A_{\text{pc}} \simeq 2 \times 10^{19} \cos(\alpha) (\dot{P}_{-15}/P^3)^{0.5} \text{ cm}^{-1}$. Here \dot{P}_{-15} is the spin down rate expressed in units of 10^{-15} s/s . The spin down energy loss can be expressed as $\dot{E} \simeq 4 \times 10^{31} (\dot{P}_{-15}/P) \text{ erg s}^{-1} \simeq \dot{E}_1 \dot{P}_{-15}/P$. The quantity $m_e c^3 \simeq 2.5 \times 10^4 \text{ erg cm s}^{-1}$.

Now we can estimate a ratio of L_{PSG} and \dot{E} as:

$$\xi = \frac{L_{\text{PSG}}}{\dot{E}} \simeq 1.2 \times 10^{-8} \eta \gamma_0 \cos(\alpha) \left(\frac{\dot{E}}{\dot{E}_1} \right)^{-0.5} \quad (11)$$

and, therefore, using Equation (9)

$$P_3 \simeq 2 \times 10^{-9} \left(\frac{\gamma_0}{\xi} \right) \left(\frac{\dot{E}}{\dot{E}_1} \right)^{-0.5}. \quad (12)$$

The parameter $\gamma_0 \sim 10^6$ and is more or less the same for most radio pulsars (Szary *et al.* 2015). We can also assume that the major part of L_{PSG} powers the thermal as well as non-thermal X-ray emission, and as was shown by Becker (2009) $\xi \simeq 10^{-3}$. Thus we can conclude that the dependence of P_3 on \dot{E} expressed by equation (12) is in agreement with the observed data as shown in figure 7 (solid line). It should be noted that there is a significant spread in ξ reported in the literature (e.g. (Kargaltsev *et al.* 2012)), and this can

cause the relation given by equation 12 to vary. A detailed study of the effect of PSG model on the drifting phenomenon will be carried out in a future work.

7. Summary and Discussion

We have carried out a detailed analysis of drifting in a large sample of pulsars observed as part of MSPES. Our fluctuation spectral analysis were able to detect periodic features in 57 pulsars including 22 pulsars where drifting was seen for the first time. The drifting was found to be broadband in nature and showed consistent features of pulsar emission like radius to frequency mapping. The pulsar population can be classified into three groups based on drifting, the pulsars with phase modulated drifting, the pulsars with amplitude modulated drifting and finally the pulsars with no drifting. The three groups show distinct distributions in terms of their \dot{E} values. The phase modulated drifting is confined to a narrow range with low \dot{E} (10^{30} - 10^{33} erg s $^{-1}$) while the pulsars with no drifting mostly have high \dot{E} values. The amplitude modulated drifting distribution peaks in the intermediate \dot{E} range. It seems likely that the pulsar energetics influence the nature of radio emission. The phase modulated drifting exhibit the most ordered emission and is associated with the least energetic pulsars, while the most energetic pulsars do not show any drifting. A study with a larger sample of pulsars would be helpful in further distinguishing the three populations. The aliasing effect introduces ambiguity in associating a periodicity to the measured peak in the fluctuation spectra. There is also the added uncertainty connected with direction of subpulse motion in the pulse window which introduces an additional two way degeneracy in estimating P_3 . However, using physical arguments about charge motion in the inner acceleration region we were able to predict the direction of subpulse motion in the pulsars showing phase modulation. The estimated P_3 in these cases showed an anti-correlation with \dot{E} , which seems to favour the Partially Screened Gap model of the inner acceleration region in pulsars. The anti-correlation also provide a natural explanation for the absence of phase modulated drifting in high energetic pulsars ($> 10^{33}$ erg s $^{-1}$) as the expected P_3 will go below P at this range.

Acknowledgments: We would like to thank Late Prof. Janusz Gil for his motivation and encouragement to embark on the subpulse drifting problem. We thank the referee Patrick Weltevrede for his comments especially on the aliasing effect which helped to improve the paper. We thank Joanna Rankin, Wojciech Lewandowski and Jarek Kijak for critical comments on the manuscript. We would like to thank staff of Giant Meter-wave Radio Telescope and National Center for Radio Astrophysics for providing valuable support in carrying out this project. This work was supported by grants DEC-2012/05/B/ST9/03924 and DEC-2013/09/B/ST9/02177 of the Polish National Science Centre. This work was financed by the Netherlands Organisation for Scientific Research (NWO) under project ‘‘CleanMachine’’ (614.001.301).

REFERENCES

- Asseo, E.; Melikidze, G.I. 1998, MNRAS, 301, 59
- Asgekar, A.; Deshpande, A.A. 2005, MNRAS, 357, 1105
- Backer, D.C. 1970, Nature, 227, 692
- Backer, D.C. 2009, Astrophysics and Space Sciences library Vol. 357, X-ray Emission from Pulsars and Neutron Stars, 91
- Backer, D.C.; Rankin, J.M.; Campbell, D.B. 1975, ApJ, 197, 481
- Backus, I.; Mitra, D.; Rankin, J.M. 2010, MNRAS, 404, 30
- Basu, R.; Mitra, D.; Melikidze, G.I. 2013, ApJ, 772, 86
- Biggs, J.D.; Hamilton, P.A.; McCulloch, P.M.; Manchester, R.N. 1985, MNRAS, 214, 47
- Biggs, J.D.; Hamilton, P.A.; McCulloch, P.M.; Manchester, R.N. 1987, MNRAS, 228, 119
- Becker, W. 2009, Ap&SS, 357, 91
- Bhattacharyya, B.; Gupta, Y.; Gil, J.; Sendyk, M. 2007, MNRAS, 377, L10
- Bhattacharyya, B.; Gupta, Y.; Gil, J. 2009, MNRAS, 398, 1435

- Deich, W.T.S.; Cordes, J.M.; Hankins, T.H.; Rankin, J.M. 1986 ApJ, 300, 540
- Deshpande, A.A.; Rankin, J.M. 1999 ApJ, 524, 1008
- Deshpande, A.A.; Rankin, J.M. 2001 MNRAS, 322, 438
- Drake, F.D.; Craft, H.D. 1968, Nature, 220, 231
- Edwards, R.T.; Stappers, B.W. 2002, A&A, 393, 733
- Force, M.M.; Rankin, J.M. 2010, MNRAS, 406, 237
- Geppert, U., Gil, J., & Melikidze, G. 2013, MNRAS, 435, 3262
- Gil, J.A.; Sendyk, M. 2000, ApJ, 541, 351
- Gil, J.A.; Mitra, D. 2001, ApJ, 550, 383
- Gil, J.A., Melikidze, G.I., & Mitra, D. 2002a, A&A, 388, 235
- Gil, J.A., Melikidze, G.I., & Mitra, D. 2002b, A&A, 388, 246
- Gil, J.; Melikidze, G.I.; Geppert, U. 2003a, A&A, 407, 315
- Gil, J.A.; Sendyk, M. 2003b, ApJ, 585, 453
- Gil, J.; Lyubarsky, Y.; Melikidze, G.I. 2004, ApJ, 600, 872
- Gil, J.; Melikidze, G.I.; Zhang, B. 2006, ChJAS, 6, 105
- Gil, J.; Haberl, F.; Melikidze, G.I.; Geppert, U.; Zhang, B.; Melikidze, G., Jr. 2008, ApJ, 686, 497
- Goldreich, P.; Julian, W.H. 1969, ApJ, 157, 869
- Gupta, Y.; Gil, J.; Kijak, J.; Sendyk, M. 2004, A&A, 426, 229
- Hankins, T.H.; Wolszczan, A. 1987, ApJ, 318, 410
- Huguenin, G.R.; Taylor, J.H.; Troland, T.H. 1970, ApJ, 162, 727
- Janssen, G.H.; van Leeuwen, J. 2004, A&A, 425, 255
- Kargaltsev, O.; Durant, M.; Pavlov, G. G.; Garmire, G. 2012, ApJS, 201, 37
- Kijak, J.; Gil, J. 1997, MNRAS, 288, 631
- Kijak, J.; Gil, J. 2003, A&A, 397, 969
- Kloumann, I.M.; Rankin, J.M. 2010, MNRAS, 408, 40
- Krzeszowski, K.; Mitra, D.; Gupta, Y.; Kijak, J.; Gil, J.; Acharyya, A. 2009, MNRAS, 393, 1617
- Maan, Y.; Deshpande, A.A. 2014, ApJ, 792, 130
- Lyne, A.G.; Ashworth, M. 1983, MNRAS, 204, 519
- Medin, Z.; Lai, D. 2007, MNRAS, 382, 1833
- Melikidze, G.I.; Gil, J.A.; Pataraya, A.D. 2000, ApJ, 544, 1081
- Mitra, D., Deshpande, A.A. 1999, A&A, 346, 906
- Mitra, D., Rankin, J.M. 2002, ApJ, 577, 322
- Mitra, D., Rankin, J.M. 2008, MNRAS, 385, 606
- Mitra, D., *et al.* 2016, submitted.
- Nowakowski, L.; Usowicz, J.; Kepa, A.; Wolszczan, A. 1982, A&A, 116, 158
- Oster, L.; Sieber, W. 1977, A&A, 58, 303
- Oster, L.; Hilton, D.A.; Sieber, W. 1977, A&A, 57, 323
- Press, W.H.; Teukolsky, S.H.; Vetterling, W.T.; Flannery, B.P. 1992, Numerical Recipes in C, Cambridge University Press
- Proszynski, M.; Wolszczan, A. 1986, ApJ, 307, 540
- Rankin, J.M. 1983, ApJ, 274, 333
- Rankin, J.M. 1986, ApJ, 301, 901
- Rankin, J.M. 1993a, ApJ, 405, 285
- Rankin, J.M.; Wolszczan, A.; Stinebring, D.R. 1988, ApJ, 324, 1048
- Rankin, J.M.; Wright, G.A.E.; Brown, A.M. 2013, MNRAS, 433, 445
- Redman, S.L.; Wright, G.A.E.; Rankin, J.M. 2005, MNRAS, 357, 859

- Ruderman, M.A.; Sutherland, P.G. 1975, ApJ, 196, 51
- Schönhardt, R.E.; Sieber, W. 1973, ApL, 14, 61
- Srostlik, Z.; Rankin, J.M. 2005, MNRAS, 362, 1121
- Serylak, M.; Stappers, B.W.; Weltevrede, P. 2009, A&A, 506, 865
- Sieber, W.; Oster, L. 1975, A&A, 38, 325
- Smits, J.M.; Mitra, D.; Kuijpers, J. 2005, A&A, 440, 683
- Spitkovsky, A. 2011, ASSP, 21, 139
- Sutton, J.M.; Staelin, D.H.; Price, R.M.; Weimer, R. 1970, ApJL, 159, L89
- Szary, A. 2013, PhD Thesis, arXiv:1304.4203.
- Szary, A., Melikidze, G.I., Gil, J. 2015, MNRAS, 447, 2295
- Taylor, J.H.; Huguenin, G.R. 1971, ApJ, 167, 273
- Taylor, J.H.; Manchester, R.N.; Huguenin, G.R. 1975, ApJ, 195, 513
- Vivekanand, M.; Joshi, B. C. 1997, ApJ, 477, 431
- Weltevrede, P.; Edwards, R. T.; Stappers, B. W. 2006, A&A, 445, 243
- Weltevrede, P.; Edwards, R. T.; Stappers, B. W. 2007, A&A, 469, 607
- Wolszczan, A. 1980, A&A, 86, 7

TABLE 3

THE TABLE SHOWS THE DETAILS OF THE MEASUREMENT OF DRIFTING FEATURES IN PULSARS. THE MEASUREMENTS INCLUDE THE PEAK FREQUENCY f_p FROM THE LONGITUDE RESOLVED FLUCTUATION SPECTRA AND THE HARMONIC RESOLVED FLUCTUATION SPECTRA, THE STRENGTH OF PEAK FEATURE QUANTIFIED BY THE PARAMETER S FOR EACH PEAK AND THE SEPARATION BETWEEN THE SUBPULSES SPECIFIED BY P_2 . COLUMN 2-6 GIVES THE MEASUREMENTS AT 333 MHz WHILE COLUMNS 7-11 GIVES THE CORRESPONDING VALUES AT 618 MHz.

PSR	333 MHz					618 MHz				
	f_p (LRFS) (cycles/P)	S (LRFS) (P)	P_2 ($^\circ$)	f_p (HRFS) (cycles/P)	S (HRFS) (P)	f_p (LRFS) (cycles/P)	S (LRFS) (P)	P_2 ($^\circ$)	f_p (HRFS) (cycles/P)	S (HRFS) (P)
J0034-0721	0.150 \pm 0.011 0.301 \pm 0.018	23.1 \pm 3.7 2.0 \pm 0.3	19.1 \pm 0.2	0.150 \pm 0.014 0.298 \pm 0.023	23.3 \pm 2.9 3.3 \pm 0.4	0.154 \pm 0.011	14.4 \pm 2.1	16.7 \pm 0.2	0.153 \pm 0.012	24.0 \pm 3.3
J0151-0635	0.067 \pm 0.004	33.8 \pm 2.7	—	0.067 \pm 0.004 0.932 \pm 0.004	75.5 \pm 5.4 25.1 \pm 2.6	0.072 \pm 0.004	56.1 \pm 3.1	—	0.072 \pm 0.004	92.6 \pm 5.5
J0152-1637	0.176 \pm 0.031	3.0 \pm 0.5	—	0.169 \pm 0.027	8.0 \pm 1.1	0.169 \pm 0.030	2.6 \pm 0.5	—	0.163 \pm 0.029	6.1 \pm 0.9
J0304+1932	0.016 \pm 0.009 0.142 \pm 0.039	17.8 \pm 3.4 2.4 \pm 0.2	—	0.020 \pm 0.011 0.158 \pm 0.045 0.986 \pm 0.046	17.7 \pm 2.7 4.7 \pm 0.3 3.3 \pm 0.3	0.157 \pm 0.039	2.7 \pm 0.2	—	0.171 \pm 0.049	3.0 \pm 0.3
J0525+1115	—	—	—	0.684 \pm 0.052	1.9 \pm 0.4	—	—	—	—	—
J0630-2834	—	—	—	—	—	0.134 \pm 0.044	1.6 \pm 0.3	—	0.855 \pm 0.032	5.1 \pm 0.7
J0758-1528	—	—	—	—	—	0.042 \pm 0.018	5.9 \pm 0.7	—	0.047 \pm 0.022 0.953 \pm 0.015	8.7 \pm 1.0 15.2 \pm 1.1
J0820-1350	0.211 \pm 0.006	61.7 \pm 2.3	4.11 \pm 0.07	0.211 \pm 0.007	59.8 \pm 2.4	0.211 \pm 0.005	65.3 \pm 1.8	3.93 \pm 0.05	0.211 \pm 0.005 0.788 \pm 0.005	69.6 \pm 2.1 7.3 \pm 1.2
J0837+0610	0.462 \pm 0.006	31.5 \pm 3.6	—	0.458 \pm 0.004	50.8 \pm 6.3	0.463 \pm 0.007	20.7 \pm 2.0	—	0.464 \pm 0.008 0.536 \pm 0.004	19.4 \pm 2.9 46.0 \pm 5.1
J0846-3533	0.493 \pm 0.006	19.4 \pm 0.5	—	0.492 \pm 0.005 0.507 \pm 0.006	51.9 \pm 1.2 28.8 \pm 1.0	0.491 \pm 0.004	17.3 \pm 0.9	—	0.492 \pm 0.005	50.8 \pm 1.9
J0944-1354	—	—	1.4 \pm 0.3	0.156 \pm 0.008	19.7 \pm 3.2	—	—	—	—	—
J0959-4809	—	—	—	—	—	—	—	—	0.179 \pm 0.041	4.2 \pm 0.4
J1034-3224	0.139 \pm 0.007	24.4 \pm 1.6	—	0.141 \pm 0.009 0.859 \pm 0.007	31.0 \pm 3.0 37.9 \pm 2.8	0.139 \pm 0.012	5.1 \pm 0.5	—	0.138 \pm 0.013 0.860 \pm 0.013	14.4 \pm 1.7 18.4 \pm 1.0
J1041-1942	—	—	—	—	—	0.233 \pm 0.024	2.5 \pm 0.3	—	—	—
J1116-4122	0.027 \pm 0.010 0.050 \pm 0.010	17.5 \pm 3.2 13.3 \pm 2.3	2.9 \pm 0.2	0.028 \pm 0.011 0.050 \pm 0.012 0.950 \pm 0.017 0.973 \pm 0.024	18.6 \pm 3.3 15.6 \pm 2.6 9.4 \pm 1.1 8.1 \pm 0.8	—	—	—	0.768 \pm 0.028	7.0 \pm 0.6

TABLE 3—Continued

PSR	333 MHz					618 MHz				
	f_p (LRFS) (cycles/P)	S (LRFS) (P)	P_2 (°)	f_p (HRFS) (cycles/P)	S (HRFS) (P)	f_p (LRFS) (cycles/P)	S (LRFS) (P)	P_2 (°)	f_p (HRFS) (cycles/P)	S (HRFS) (P)
J1239+2453	0.361±0.011	18.0±1.2	—	0.360±0.015	19.0±1.6	0.361±0.014	15.6±1.0	—	0.361±0.019	14.3±1.5
	—	—	—	0.639±0.011	24.6±1.8	—	—	—	0.639±0.010	30.1±2.6
J1328–4921	0.296±0.018	8.5±0.7	—	0.296±0.018	16.5±1.4	0.294±0.017	4.8±0.4	—	0.291±0.018	16.1±1.1
	—	—	—	0.705±0.019	15.6±1.0	—	—	—	0.706±0.018	12.5±0.6
J1418–3921	—	—	—	—	—	0.400±0.004	23.2±1.8	—	—	—
	—	—	—	—	—	—	—	—	0.598±0.005	50.3±3.4
J1527–3931	0.026±0.004	33.5±6.2	—	—	—	—	—	—	—	—
	—	—	—	0.975±0.004	59.7±9.8	—	—	—	—	—
J1555–3134	0.053±0.012	13.5±1.9	—	0.053±0.012	24.3±3.3	0.055±0.010	16.7±2.7	—	0.055±0.012	24.8±3.6
	0.096±0.008	18.3±1.6	—	0.096±0.010	27.0±3.0	0.098±0.008	21.9±1.8	—	0.098±0.008	35.6±3.3
	—	—	—	0.902±0.012	7.4±0.6	—	—	—	—	—
	—	—	—	0.949±0.013	8.5±0.5	—	—	—	0.947±0.013	8.5±0.4
J1603–2531	—	—	—	—	—	0.015±0.006	16.8±4.6	—	0.014±0.006	24.6±7.3
	—	—	—	—	—	—	—	—	0.986±0.009	14.9±2.1
J1604–4909	—	—	—	—	—	0.020±0.011	8.4±1.5	—	0.020±0.010	21.3±4.3
	—	—	—	—	—	—	—	—	0.980±0.016	13.2±1.5
J1625–4048	—	—	—	—	—	0.017±0.010	3.3±0.5	—	0.016±0.010	17.3±2.3
	—	—	—	—	—	—	—	—	0.983±0.010	22.3±1.2
J1645–0317	—	—	—	—	—	0.080±0.030	4.9±0.6	—	0.080±0.027	7.3±1.0
	—	—	—	—	—	—	—	—	0.924±0.025	7.1±1.0
J1700–3312	—	—	—	—	—	0.444±0.020	1.3±0.3	—	—	—
	—	—	—	—	—	—	—	—	0.553±0.022	6.5±0.9
J1703–3241	0.212±0.031	3.8±0.3	—	0.215±0.029	5.7±0.7	0.211±0.022	6.5±0.5	—	0.216±0.022	5.5±0.7
	—	—	—	0.814±0.055	4.0±0.3	—	—	—	0.792±0.027	8.7±0.5
J1720–2933	0.408±0.003	90.5±1.0	10.1±0.3	0.408±0.004	102.0±1.2	0.409±0.003	88.2±1.0	8.8±0.3	0.409±0.004	98.4±1.2
	0.183±0.004	9.5±0.6	7.8±0.3	—	—	0.183±0.003	17.8±0.9	—	—	—
	—	—	—	0.592±0.003	11.1±0.9	—	—	—	0.589±0.004	7.5±0.8
	—	—	—	0.817±0.004	19.4±0.7	—	—	—	0.817±0.004	31.3±0.8
J1722–3207	—	—	—	—	—	0.044±0.023	2.2±0.3	—	0.044±0.016	9.7±1.4
	—	—	—	—	—	—	—	—	0.958±0.019	7.3±0.7

TABLE 3—Continued

PSR	333 MHz				618 MHz			
	f_p (LRFS) (cycles/P)	S (LRFS) (P)	P_2 ($^\circ$)	f_p (HRFS) (cycles/P)	S (HRFS) (P)	P_2 ($^\circ$)	f_p (LRFS) (cycles/P)	S (LRFS) (P)
J1733–2228	0.038±0.025	4.1±0.3	—	0.039±0.025 0.973±0.017	12.5±0.8 12.4±0.4	—	0.048±0.029	0.9±0.1
J1733–3716	—	—	—	—	—	—	0.013±0.004	5.9±2.2
J1735–0724	0.053±0.019	10.5±1.2	—	0.052±0.024 0.949±0.017	8.2±1.0 14.6±1.1	—	0.046±0.023	3.3±0.4
J1740+1311	—	—	—	—	—	—	0.113±0.029	3.6±0.3
J1741–3927	0.029±0.017	3.6±0.4	—	—	—	—	0.105±0.052 0.015±0.010	2.0±0.2 13.0±2.5
J1741–0840	0.211±0.029	3.3±0.3	—	0.779±0.023 0.036±0.002 0.965±0.001	4.8±0.4 20.4±4.1 11.9±9.4	—	0.206±0.026	3.2±0.3
J1748–1300	0.148±0.012	4.7±0.6	—	0.153±0.017 0.851±0.015	9.7±1.4 10.2±1.2	—	—	—
J1801–0357	0.012±0.006	28.4±7.8	—	0.012±0.006 0.988±0.006	40.4±11.0 38.9±2.4	—	0.013±0.006	30.5±9.2
J1801–2920	—	—	—	—	—	—	0.404±0.013	4.1±0.7
J1816–2650	0.245±0.011	1.8±0.3	—	0.240±0.025	9.3±0.9	—	—	—
J1822–2256	0.059±0.008	18.1±2.5	8.6±0.2	0.060±0.009	35.6±5.6	7.1±0.2	0.057±0.007	26.4±3.3
J1842–0359	0.082±0.004	4.7±0.8	—	0.082±0.004	63.1±4.6	—	0.080±0.003 0.058±0.004 0.036±0.006 0.161±0.007	54.1±2.0 11.8±1.0 5.7±1.0 3.0±0.4
	—	—	—	0.919±0.004	38.6±3.6	—	—	—
	—	—	—	—	—	—	0.920±0.003 0.943±0.005	107.6±2.6 20.8±1.4

TABLE 3—Continued

PSR	333 MHz				618 MHz					
	f_p (LRFS) (cycles/P)	S (LRFS) (P)	P_2 ($^\circ$)	f_p (HRFS) (cycles/P)	S (HRFS) (P)	f_p (LRFS) (cycles/P)	S (LRFS) (P)	P_2 ($^\circ$)	f_p (HRFS) (cycles/P)	S (HRFS) (P)
J1848–0123	—	—	—	—	—	—	—	—	0.84±0.008	8.4±0.8
	—	—	—	—	—	0.051±0.018	4.3±0.5	—	0.049±0.022 0.949±0.014	7.2±0.8 17.5±0.9
J1900–2600	—	—	—	0.135±0.023 0.866±0.023	7.4±1.0 8.0±0.9	0.129±0.011	14.1±1.9	—	0.136±0.020 0.869±0.021	8.2±1.2 9.2±0.9
J1901–0906	0.327±0.011 0.138±0.017 0.190±0.007	14.7±0.6 8.0±0.6 6.3±0.5	—	0.325±0.012 0.137±0.011 0.189±0.011	29.6±1.2 10.0±0.9 6.2±0.6	0.329±0.008 0.135±0.011 0.195±0.010	17.9±0.7 4.8±0.6 5.4±0.5	—	0.328±0.010 0.138±0.011 0.194±0.012	35.2±1.4 11.1±1.2 7.4±0.9
	—	—	—	0.667±0.011 0.809±0.007	12.5±0.5 7.1±0.7	—	—	—	0.671±0.009 0.809±0.012	11.9±1.0 6.1±0.8
J1909+1102	0.078±0.017	7.8±0.9	—	0.073±0.014 0.926±0.025	15.2±2.2 6.9±0.6	0.065±0.029	3.9±0.4	—	0.055±0.024 0.932±0.032	7.4±1.0 5.0±0.7
J1919+0021	0.091±0.003	71.8±6.2	—	0.091±0.006 0.909±0.003	86.7±8.3 99.1±7.6	—	—	—	—	—
J1919+0134	—	—	—	—	—	0.153±0.013	2.5±0.3	—	0.152±0.014	18.8±1.9
J1921+1948	0.168±0.007	4.8±0.4	—	0.834±0.007 0.736±0.017	36.2±1.5 8.6±0.6	—	—	—	—	—
J1921+2153	—	—	—	—	—	0.236±0.013	12.8±0.9	—	0.235±0.014 0.764±0.012	22.1±1.4 9.8±0.7
J1932+1059	0.087±0.010	16.3±2.3	—	0.087±0.010 0.913±0.010	17.6±2.6 17.3±1.6	—	—	—	—	—
J1946+1805	—	—	12.9±0.8	—	—	0.036±0.003	101.5±9.2	9.2±0.4	0.037±0.003 0.966±0.003 0.986±0.003	127.7±10.6 99.2±4.2 77.4±3.8
J2006–0807	0.027±0.008 0.065±0.017	10.0±2.1 3.2±0.4	—	0.027±0.008 0.066±0.011 0.973±0.007	24.9±5.7 15.4±2.6 21.2±1.9	0.017±0.003	31.3±6.7	—	0.017±0.005	61.9±18.0
J2046–0421	0.363±0.005	56.5±1.5	3.37±0.06	—	—	0.364±0.004	60.5±1.8	3.15±0.04	0.982±0.004	58.9±4.2
	—	—	—	0.637±0.006	54.6±1.4	—	—	—	0.635±0.005	71.0±1.7

TABLE 3—*Continued*

PSR	333 MHz				618 MHz					
	f_p (LRFS) (cycles/P)	S (LRFS) (P)	P_2 ($^\circ$)	f_p (HRFS) (cycles/P)	S (HRFS) (P)	f_p (LRFS) (cycles/P)	S (LRFS) (P)	P_2 ($^\circ$)	f_p (HRSF) (cycles/P)	S (HRFS) (P)
J2046+1540	—	—	—	—	—	0.043 \pm 0.011 0.107 \pm 0.022	4.1 \pm 0.7 1.1 \pm 0.2	—	0.044 \pm 0.012 0.108 \pm 0.023	18.5 \pm 2.8 6.7 \pm 0.8
J2048–1616	0.310 \pm 0.003	64.9 \pm 9.2	—	0.310 \pm 0.003 0.691 \pm 0.002	65.8 \pm 7.0 80.7 \pm 10.1	—	—	—	—	—
J2305+3100	0.485 \pm 0.010	26.0 \pm 0.7	4.5 \pm 0.3	— 0.513 \pm 0.011	— 30.4 \pm 0.9	—	—	—	—	—
J2317+2149	0.191 \pm 0.021	3.7 \pm 0.8	2.2 \pm 0.3	0.190 \pm 0.030	13.8 \pm 1.9	0.194 \pm 0.019	2.1 \pm 0.4	2.6 \pm 0.2	0.193 \pm 0.010	15.8 \pm 1.9
J2330–2005	0.044 \pm 0.018	13.3 \pm 1.4	—	0.041 \pm 0.015 0.957 \pm 0.021	16.8 \pm 2.5 12.1 \pm 1.1	—	—	—	—	—

TABLE 4

THE TABLE PRESENTS THE ESTIMATED DRIFTING PROPERTIES ALONG WITH PHYSICAL PARAMETERS FOR THE PULSARS. COLUMN 2 AND 3 PRESENT THE PERIOD AND \dot{E} OBTAINED FROM THE ATNF PULSAR DATABASE. COLUMN 4 PRESENTS THE TYPE OF DRIFTING FROM THREE POSSIBILITIES, ND - NEGATIVE DRIFTING, PD - POSITIVE DRIFTING AND AMD - AMPLITUDE MODULATED DRIFTING. THE PULSAR J1034–3224 SHOWED A COMPLEX PHASE BEHAVIOUR WHICH COULD NOT BE CATEGORIZED INTO ANY OF THE THREE FORMS. COLUMN 5 PRESENTS THE PEAK FREQUENCY (f_p) OF DRIFTING. THE f_p IS THE WEIGHTED AVERAGE OF THE MEASUREMENTS OVER THE TWO OBSERVING FREQUENCIES AS WELL AS THE LRFS AND HRFS, SEE TABLE ?? FOR INDIVIDUAL MEASUREMENTS. IN CASE OF MULTIPLE PEAKS FOR A GIVEN PULSAR WE HAVE ONLY USED THE MOST SIGNIFICANT PEAK. THE TWO PULSARS J1116–4122 AND J1555–3134 HAD TWO PEAKS WITH EQUIVALENT S AND BOTH WERE REPORTED. THE PD HAS $0.5 < f_p < 1$ CYCLES/ P WHILE FOR ND AND AMD $0 < f_p < 0.5$ CYCLES/ P , SEE TEXT FOR DETAIL. COLUMN 6 PRESENTS THE ESTIMATED DRIFT PERIODICITY $P_3 = 1/f_p$.

PSR	P (s)	\dot{E} (10^{30} erg s $^{-1}$)	Type	f_p (cycles/ P)	P_3 (P)
J0034–0721	0.9430	19.2	ND	0.152±0.012	6.6±0.5
J0151–0635	1.4647	5.56	ND	0.0695±0.004	14.4±0.8
J0152–1637	0.8327	88.8	ND	0.169±0.029	5.9±1.0
J0304+1932	1.3876	19.1	ND	0.155±0.042	6.4±1.7
J0525+1115	0.3544	65.3	PD	0.684±0.052	1.5±0.1
J0630–2834	1.2444	146	PD	0.855±0.032	1.17±0.04
J0758–1528	0.6823	201	AMD	0.044±0.020	22.7±10.1
J0820–1350	1.2381	43.8	ND	0.211±0.006	4.7±0.1
J0837+0610	1.2738	130	AMD	0.460±0.005	2.17±0.03
J0846–3533	1.1161	45.5	ND	0.492±0.005	2.03±0.02
J0944–1354	0.5703	9.63	ND	0.156±0.008	6.4±0.3
J0959–4809	0.6701	10.8	ND	0.179±0.041	5.6±1.3
J1034–3224	1.1506	5.97	—	0.139±0.009	7.2±0.5
J1041–1942	1.3864	14.0	ND	0.233±0.024	4.3±0.4
J1116–4122	0.9432	374	AMD	0.028±0.011 0.050±0.011	36.4±13.9 20.0±4.3
J1239+2453	1.3824	14.3	AMD	0.361±0.014	2.8±0.1
J1328–4921	1.4787	7.45	AMD	0.294±0.018	3.4±0.2
J1418–3921	1.0968	26.6	PD	0.598±0.005	1.67±0.01
J1527–3931	2.4176	53.3	PD	0.975±0.004	1.026±0.004
J1555–3134	0.5181	17.7	ND	0.097±0.008 0.054±0.011	10.3±0.9 18.5±3.9
J1603–2531	0.2831	2.77×10 ³	AMD	0.0145±0.006	69.0±28.5

TABLE 4—*Continued*

PSR	P (s)	\dot{E} (10^{30}erg s^{-1})	Type	f_p (cycles/ P)	P_3 (P)
J1604–4909	0.3274	1.15×10^3	AMD	0.020 ± 0.010	50.0 ± 26.1
J1625–4048	2.3553	1.34	AMD	0.0165 ± 0.010	60.6 ± 36.7
J1645–0317	0.3877	1.21×10^3	AMD	0.080 ± 0.028	12.5 ± 4.4
J1700–3312	1.3583	74.2	PD	0.553 ± 0.022	1.81 ± 0.07
J1703–3241	1.2118	14.6	PD	0.214 ± 0.025	4.7 ± 0.5
J1720–2933	0.6204	123	ND	0.4085 ± 0.003	2.45 ± 0.02
J1722–3207	0.4772	235	AMD	0.044 ± 0.018	22.7 ± 9.4
J1733–2228	0.8717	2.55	AMD	0.044 ± 0.026	22.9 ± 13.7
J1733–3716	0.3376	1.54×10^4	AMD	0.014 ± 0.004	71.4 ± 20.4
J1735–0724	0.4193	650	AMD	0.051 ± 0.019	19.7 ± 7.5
J1740+1311	0.8030	111	AMD	0.113 ± 0.029	8.8 ± 2.3
J1741–3927	0.5122	567	AMD	0.106 ± 0.047	9.5 ± 4.2
J1741–0840	2.0431	10.5	PD	0.782 ± 0.027	1.28 ± 0.04
J1748–1300	0.3941	782	AMD	0.150 ± 0.014	6.7 ± 0.6
J1801–0357	0.9215	167	AMD	0.012 ± 0.006	81.4 ± 41.9
J1801–2920	1.0819	103	AMD	0.404 ± 0.013	2.48 ± 0.08
J1816–2650	0.5929	12.6	ND	0.244 ± 0.013	4.1 ± 0.2
J1822–2256	1.8743	8.12	ND	0.058 ± 0.008	17.2 ± 2.3
J1842–0359	1.8399	3.22	AMD	0.081 ± 0.003	12.4 ± 0.5
J1848–0123	0.6594	723	AMD	0.050 ± 0.020	19.9 ± 7.8
J1900–2600	0.6122	35.2	AMD	0.131 ± 0.015	7.6 ± 0.8

TABLE 4—*Continued*

PSR	P	\dot{E}	Type	f_p	P_3
	(s)	(10^{30} erg s $^{-1}$)		(cycles/ P)	(P)
J1901–0906	1.7819	11.4	ND	0.328±0.010	3.05±0.09
J1909+1102	0.2836	4.57×10 ³	AMD	0.071±0.018	14.1±3.6
J1919+0021	1.2723	147	AMD	0.091±0.004	11.0±0.4
J1919+0134	1.6040	5.63	ND	0.153±0.013	6.6±0.6
J1921+1948	0.8210	63.9	PD	0.834±0.007	1.20±0.01
J1921+2153	1.3373	22.3	ND	0.236±0.013	4.2±0.2
J1932+1059	0.2265	3.93×10 ³	AMD	0.087±0.010	11.5±1.3
J1946+1805	0.4406	11.1	AMD	0.0365±0.003	27.4±2.3
J2006–0807	0.5809	9.27	AMD	0.019±0.004	53.4±12.3
J2046–0421	1.5469	15.7	PD	0.636±0.005	1.57±0.01
J2046+1540	1.1383	4.88	ND	0.043±0.011	23.0±6.1
J2048–1616	1.9616	57.3	AMD	0.310±0.003	3.23±0.03
J2305+3100	1.5759	29.2	PD	0.513±0.011	1.95±0.04
J2317+2149	1.4447	13.7	ND	0.193±0.014	5.2±0.4
J2330–2005	1.6436	41.2	AMD	0.042±0.016	23.7±9.1

We have made the plots and data products from our survey freely available to the user. Several of the data products for each pulsar have been archived in the website:
<http://mspes.ia.uz.zgora.pl/>

The bulk download of fluctuation spectra figures for each pulsar is available from:
<ftp://ftpkn.nrao.tifr.res.in/dmitra/MSPES/MSPESII>

A. Initial data Processing

A.1. Correcting for baseline variations

The time series data had a background level which varied due to systematics in the telescope system with the possibility of giving rise to spurious periodicities in the drifting analysis. As a first step we intended to remove the background level with systematics in the baseline without affecting any intrinsic periodicity in the pulse sequence. The time series was folded using the periodicity of the pulsar and the pulse window (W_p) was determined. A running mean across the time series was calculated, excluding the pulse window, with a mean value set up for roughly every tenth part of the pulsar period. A running polynomial fitting function (4^{th} order) was determined using the running mean data which served as the model for baseline. Finally, the time series data was modified by subtracting the baseline level calculated for every data point from the fitted polynomial function. This resulted in the data with mean baseline level around zero and mostly free of any spurious periodicity.

A.2. Creating pulse stack

In order to carry out the various drifting analysis the time series data had to be converted into a pulse stack. The pulse stack is a two dimensional data form, in contrast with the one dimensional time series, where the horizontal axis corresponds to the pulse number and the vertical axis the pulsar longitude. Since, the pulsar period is not necessarily an integral multiple of time resolution of observation the generation of pulse stack involved re-sampling the time series data. The pulsar period was sampled into an appropriate number of bins (n_p) and the time series data was rearranged to fill up the bins for every period. The data along any bin corresponded to a particular longitude (the entire period represents a cycle of 360°). The data could now be identified as S_{ij} , where i is the index for the period number and j corresponds to the bin number. The pulsar profile was constructed by averaging over the period along the bins, i.e.

$$p_j = \frac{1}{N} \sum_{i=1}^N S_{ij}, \quad (\text{A1})$$

where N is number of pulses. The pulse window (W_p), bound by the start and end bins, was determined as the region above the 5σ level from the baseline in the average profile (p_j).

A.3. Removing RFI and normalization

The final step in this round of data processing was to identify and edit out data affected by RFI. An off-pulse region was identified outside W_p and the mean (μ_i) and rms (σ_i) was calculated in the off-pulse region for each pulse. The statistics of the σ_i was determined across all the pulses and outliers were identified. For the subsequent drifting analysis the time ordering of the pulses needed to be preserved so the outlier pulses (with high value of σ_i and as a consequence RFI affected) were edited out by replacing all the entries in their bins with zeros. The pulsar profile p_j was once again determined after excluding all the pulses affected by

RFI and the peak value of the profile p_j^{max} was determined. All the data points S_{ij} were divided by p_j^{max} to normalize the average peak value to unity.

B. Aliasing in Subpulse Drifting

In order to demonstrate the aliasing effect in pulsars we simulated a series of single pulses using the model of (Gil & Sendyk 2003b) to reproduce the drifting phenomenon. Additionally we have also added gaussian random noise to the simulated single pulses to resemble observations. The model enabled us to select the drift periodicity P_3 as well as the direction of subpulse motion across the pulse window. We reproduced the three unique drift categories, the negative drifting (ND, figure 8, left panel), the positive drifting (PD, figure 8, central panel) and the amplitude modulated drifting (AMD, figure 8, right panel). The AMD was simulated as a special geometric configuration where the line of sight traversed the centre of the emission beam. In each case we carried out the fluctuation spectral analysis on the simulated data. We explain the result of our analysis for each of these configurations.

Phase modulation, positive slope : As explained in the main text the aliasing effect makes it impossible to distinguish between two periodicities P_3 and \bar{P}_3 from the measured peak in the fluctuation spectra, f_p , where the periodicities are $P_3 = 1/f_p$ and $\bar{P}_3 = 1/(1-f_p)$, since there is no way to distinguish whether the subpulses are moving from trailing to leading edge of the profile or vice versa. In order to demonstrate this we simulated two separate sets of single pulses with the first set having $P_3 = 2.5 P$ and the subpulses moving from the trailing to the leading edge. The second case have periodicity $P_3 = 1.67 P$, with the subpulses moving from the leading to the trailing edge. In both these cases the expected $f_p = 0.4 \text{ cycle}/P$ in LRFS as well as HRFS. The fluctuation spectra was determined for the two datasets and shown in figure 9. The measured peak in the fluctuation spectra is $f_p = 0.398 \text{ cycle}/P$. In addition the second and third order harmonics are seen in the LRFS and HRFS in both cases, implying that for these two different drifting behaviour the fluctuation spectra is indistinguishable.

Phase modulation, negative slope : We carried out simulations to demonstrate that the fluctuation spectral analysis is identical for drifting periodicities P_3 and \bar{P}_3 given the subpulses are moving in opposite directions across the pulse window in the two cases. Two separate sets of single pulses were generated with the first set having $P_3 = 2.5 P$ and the subpulses moving from the leading to the trailing edge. The second case have periodicity $P_3 = 1.67 P$, with the subpulses moving from the trailing to the leading edge. The expected $f_p = 0.4 \text{ cycle}/P$ in the LRFS and $f_p = 0.6 \text{ cycle}/P$ in the HRFS (the negative slope is expected to shift the peak in the 0.5-1 cycle/ P range in HRFS). The fluctuation spectra was determined for the two datasets and shown in figure 10. The measured peak in the fluctuation spectra is $f_p = 0.398 \text{ cycle}/P$ for the LRFS and $f_p = 0.602 \text{ cycle}/P$ for the HRFS in both configurations. In addition the second and third order harmonics are seen in the LRFS and HRFS in both cases, implying that for these two different drifting behaviour the fluctuation spectra is indistinguishable.

Amplitude modulation : We explore the implication of the subpulses moving with drift periodicities P_3 and \bar{P}_3 on the fluctuation spectra. This corresponds to a specific geometric realization where the line of sight traverses the centre of the emission beam. We have assumed the subpulses to be symmetric in structure. In this scenario the observed intensity changes as the subpulses move across the line of sight with maximum intensity when the line of sight cuts the central part of the subpulse and the intensity diminishes towards the edges. The aliasing uncertainty once again comes into play as the $P_3 > 2P$ catches the subpulse as it is leaving the line of sight which is identical to the $P_3 < 2P$ case when the subpulse is entering the line of sight. We have simulated a double peaked pulse profile with the subpulses moving from above to below in the left component and the opposite sense in the right component. We generated two datasets of single pulses with the first set having $P_3 = 2.5 P$ and the second with periodicity $P_3 = 1.67 P$. The fluctuation spectra was

determined for the two datasets and shown in figure 11. The measured peak in the fluctuation spectra is $f_p = 0.398$ cycle/ P in the LRFS in both cases. In the HRFS there were two strong peaks at $f_p = 0.398$ cycle/ P and $\bar{f}_p = 0.602$ cycle/ P . Depending on the configuration one of the peaks in the HRFS was slightly stronger than the other, but in actual observations with much more noisy data these height differences will not be measurable. One additional level of degeneracy in the amplitude modulation case is that the results are independent of the direction of subpulse motion, i.e whether the subpulses cross the line of sight from below to above or vice versa. This is highlighted by the two separate components which have opposite sense of subpulse motion but still show the same frequency peak in the fluctuation spectra.

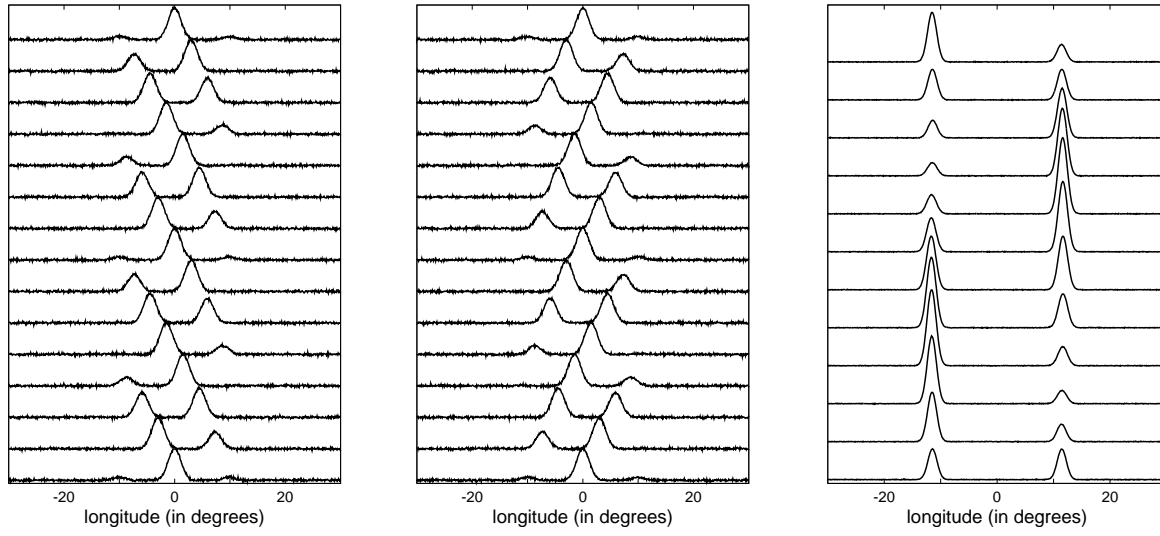


Fig. 8.— The series of simulated single pulses show the three distinct kinds of drifting phenomenon seen in pulsars. The left panel shows successive pulses appearing at slightly earlier longitudes within the pulse window and corresponds to phase modulated drifting with positive slope (ND). The central panel shows the successive pulses appearing at slightly later longitudes within the pulse window and corresponds to the phase modulated drifting with negative slope (PD). The right panel corresponds to the case of amplitude modulation (AMD) where the subpulses do not show any motion across the pulse window but periodic changes in amplitude.

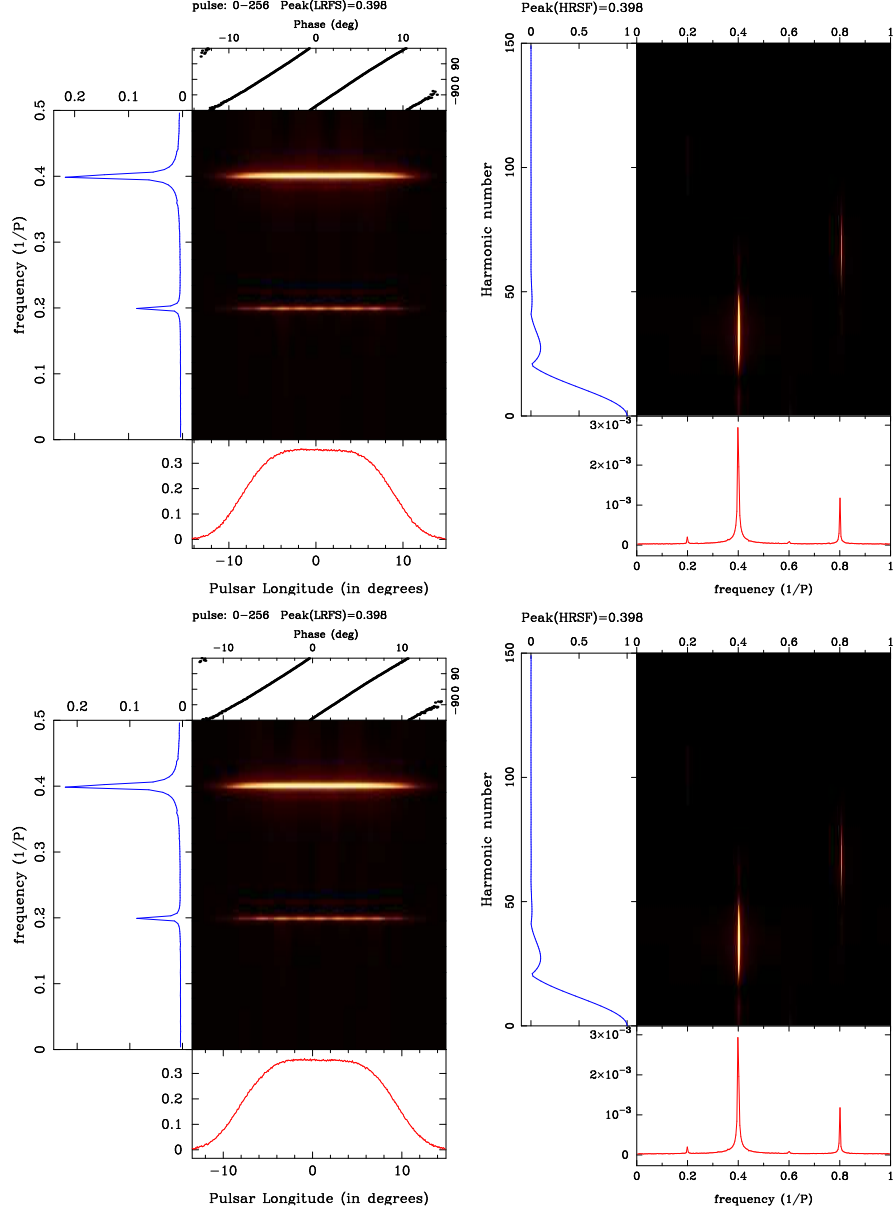


Fig. 9.— The figure show the fluctuation spectral analysis for two simulated data of phase modulated subpulse drifting with positive slope across the pulse window. The upper panel corresponds to the LRFS (top left) and HRFS (top right) for a drifting periodicity of $P_3 = 2.5 P$ and the subpulses moving from the trailing to the leading edge of the profile. The plots on the lower panel is the corresponding LRFS (bottom left) and HRFS (bottom right) for the drifting periodicity $P_3 = 1.67 P$ and the subpulses moving from the leading to the trailing edge of the profile. The measured peaks from fluctuation spectra is $f_p = 0.398 \text{ cycle}/P$ in both the data sets including identical second and third harmonics.

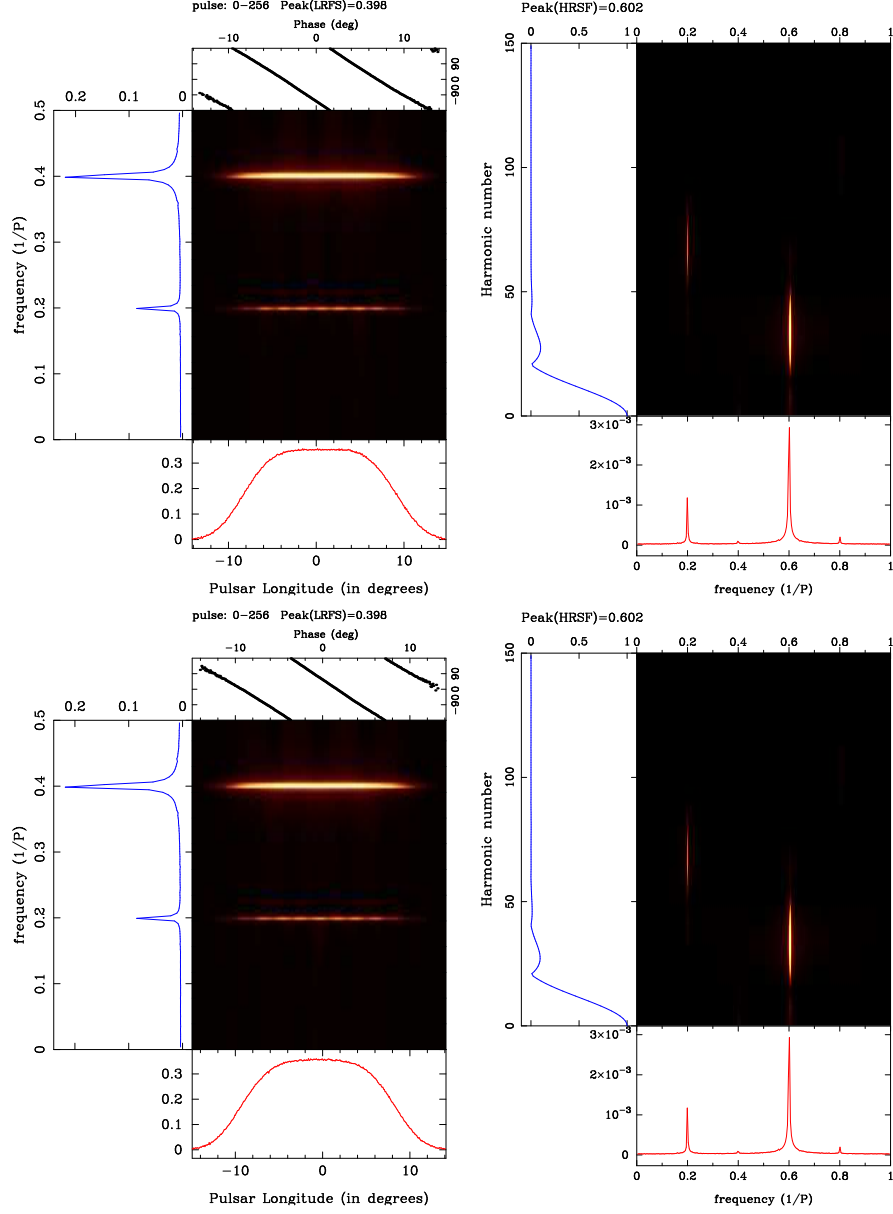


Fig. 10.— The figure show the fluctuation spectral analysis for two simulated data of phase modulated subpulse drifting with negative slope across the pulse window. The upper panel corresponds to the LRFS (top left) and HRFS (top right) for a drifting periodicity of $P_3 = 2.5 P$ and the subpulses moving from the leading to the trailing edge of the profile. The plots on the lower panel is the corresponding LRFS (bottom left) and HRFS (bottom right) for the drifting periodicity $P_3 = 1.67 P$ and the subpulses moving from the trailing to the leading edge of the profile. The measured peaks from fluctuation spectra is $f_p = 0.398 \text{ cycle}/P$ for the LRFS and $f_p = 0.602 \text{ cycle}/P$ in the HRFS for both the data sets including identical second and third harmonics.

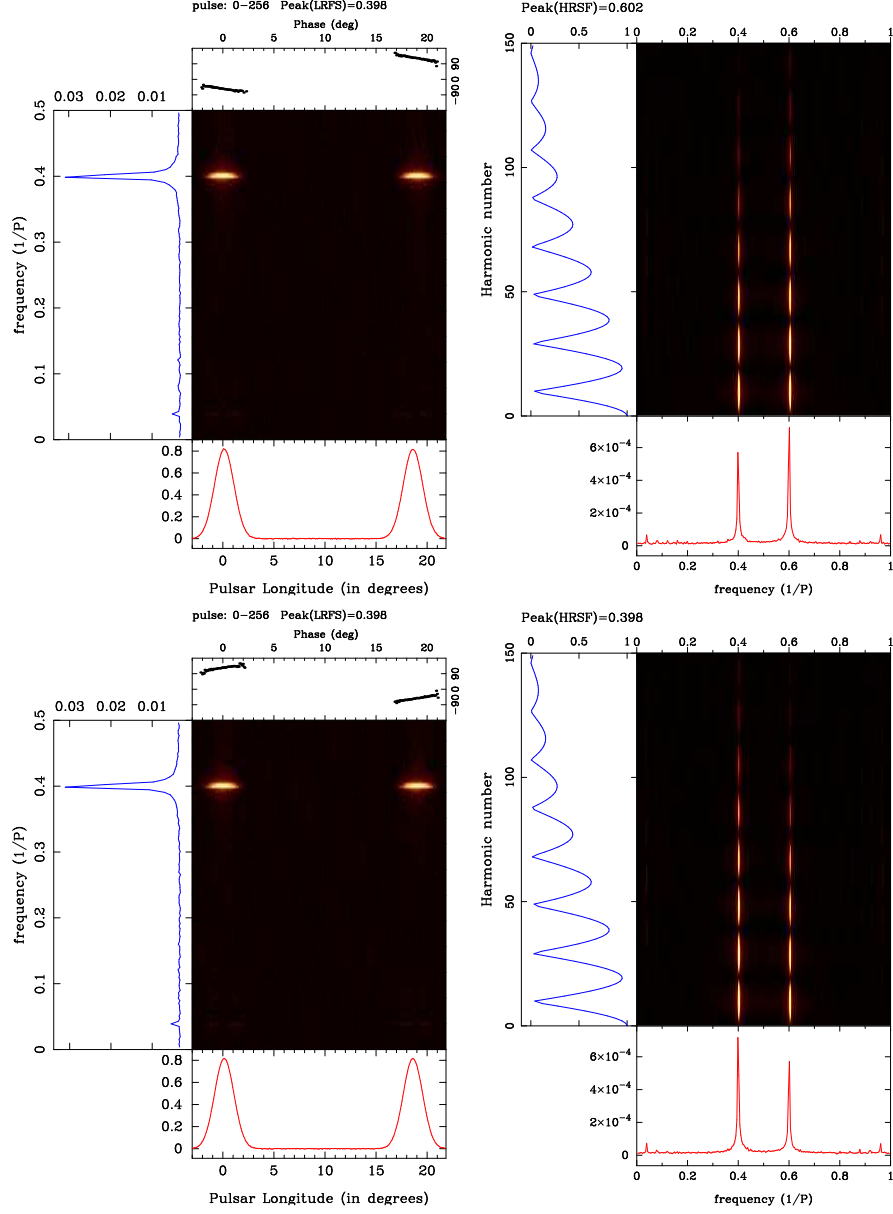


Fig. 11.— The figure show the fluctuation spectral analysis for two simulated data of amplitude modulated subpulse drifting with no subpulse motion across the pulse window. The subpulses traverse orthogonal to the line of sight with steady drift periodicities. The upper panel corresponds to the LRFS (top left) and HRFS (top right) for a drifting periodicity of $P_3 = 2.5 P$ while the plots on the lower panel is the corresponding LRFS (bottom left) and HRFS (bottom right) for the drifting periodicity $P_3 = 1.67 P$. The measured peaks from fluctuation spectra is $f_p = 0.398$ cycle/ P in the LRFS, while the HRFS show two strong peaks at $f_p = 0.398$ cycle/ P and $\tilde{f}_p = 0.602$ cycle/ P .